FINAL REPORT
FOR
SEMICONDUCTOR QUANTUM-WELL LASERS AND ULTRAFAST OPTOELECTRONIC DEVICES

May 20, 1993 – September 30, 1996

Submitted to

Dr. Yoon-Soo Park
CODE 312
Office of Naval Research
800 N. Quincy Street
Arlington, VA 22217-5660

Grant No. N00014-93-1-0844

Prepared by

S. L. Chuang
Electromagnetics Laboratory
Department of Electrical and Computer Engineering
University of Illinois
Urbana, IL 61801

September 30, 1996

DISCLAIMER NOTICE

THIS DOCUMENT IS BEST QUALITY AVAILABLE. THE COPY FURNISHED TO DTIC CONTAINED A SIGNIFICANT NUMBER OF PAGES WHICH DO NOT REPRODUCE LEGIBLY.

REPORT DOCUMENTATION PAGE

FORM APPROVED
OMB No. 0704-0188

1. AGENCY USE ONLY (Leave blank)	2. REPORT DATE	3. REPORT TYPE AND DATES COVERED
	December 1996	Final Report 21 May 1993–30 Sept 1996

4. TITLE AND SUBTITLE OF REPORT

Semiconductor Quantum-Well Lasers and Ultrafast Optoelectronic Devices

5. FUNDING NUMBERS

N00014-93-1-0844
RT & Project: 414w001-05

6. AUTHOR(s)

S. L. Chuang

7. PERFORMING ORGANIZATION NAME(S) AND ADDRESS(ES)

University of Illinois
Department of Electrical and Computer Engineering
1406 West Green
Urbana, IL 61801

8. PERFORMING ORGANIZATION REPORT NUMBER:

9. SPONSORING/MONITORING AGENCY NAME(S) AND ADDRESS(ES)

Office of Naval Research
CODE 2511:CLW
Ballston Tower One
800 North Quincy Street
Arlington, VA 22217-5660

10. SPONSORING/MONITORING AGENCY REPORT NUMBER:

11. SUPPLEMENTARY NOTES:

12a. DISTRIBUTION AVAILABILITY STATEMENT

12b. DISTRIBUTION CODE

13. ABSTRACT (Maximum 200 words)

We investigate both theoretically and experimentally high-speed strained semiconductor lasers. We have developed a systematic experimental procedure to obtain the key high-speed parameters of a semiconductor laser based on a measurement of the amplified spontaneous emission of a laser biased below threshold. We extract the gain, refractive index change, and linewidth enhancement factor spectra and compare with a complete theoretical model for the optical properties of strained semiconductors with excellent agreement. We also extend our measurement techniques to distributed-feedback lasers and show that by a careful use of both theory and experiment we can obtain these device parameters along with the important distributed feedback cavity parameters.

14. SUBJECT TERMS	15. NUMBER OF PAGES:
strained semiconductor lasers, high-speed semiconductor lasers, semiconductor laser gain, refractive index change, linewidth enhancement factor, distributed feedback lasers, InGaAsP/ InGaAs material system	26
	16. PRICE CODE

17. SECURITY CLASSIFICATION OF REPORT	18. SECURITY CLASSIFICATION OF THIS PAGE	19. SECURITY CLASSIFICATION OF ABSTRACT	20. LIMITATION OF ABSTRACT
Unclassified	Unclassified	Unclassified	UL

FINAL REPORT on AASERT Project
(May 20, 1993 – September 30, 1996)

1. **Contract Title:** Semiconductor Quantum-Well Lasers and Ultrafast Optoelectronic Devices

   Number: N00014-93-1-0844

   PI: Professor S. L. Chuang
   University of Illinois at Urbana-Champaign
   Department of Electrical and Computer Engineering
   1406 W. Green Street, Urbana, IL 61801
   Phone: (217)333-3359 Fax:(217)333-5701
   e-mail: s-chuang@uiuc.edu

   Program Manager: Dr. Y. S. Park, Code: ONR 312

2. **Technical Objectives:**

We investigated both the theoretical and experimental aspects of the ultrafast optoelectronic properties of semiconductor quantum-well lasers. Using our models, we analyzed the performance of high-speed quantum-well lasers, including distributed-feedback lasers for optical communication systems.

3. **Approach:**

   a. Development of a comprehensive theoretical model for the amplified spontaneous emission (ASE), gain, and refractive index change spectra of a strained InGaAsP quantum-well laser, designed for applications in long-wavelength communication systems.

   b. Development of an experimental system to measure these modeled spectra and to extract the linewidth enhancement factor from the ASE spectrum of a Fabry-Perot (FP) strained quantum-well semiconductor laser.

   c. Extension of our model and measurements to distributed-feedback (DFB) strained quantum-well semiconductor lasers for low-chirp, high-speed operation.

4. **Accomplishments:**

Our accomplishments include the following:

a) We have established an experimental setup and procedure for the systematic characterization of key semiconductor laser device parameters. The material gain spectrum is obtained from the maximum and minimum envelopes of the ASE spectrum, based on the Hakki-Paoli method. The refractive index change with injection current is obtained from the ASE mode positions. Finally, the linewidth enhancement factor is extracted as the ratio of the change in gain to the change in refractive index [Publication 1].

b) We have developed a comprehensive theoretical model for these device parameters including the realistic valance-band structure, and band-gap renormalization [Publications 1-3].

c) We have compared the theoretical spectra with the experimental data and demonstrated that our laser gain model is one of the few which can explain the measured spectra [Publications 1 and 2].

d) We have developed a model for the amplified spontaneous emission from a DFB semiconductor laser. We have also applied our techniques to extract the key laser performance parameters as well as cavity parameters from a DFB laser. We have found that it is necessary to use a careful combination of both theory and experiment to extract these spectra [Publications 2, 4 and 5].

5. Significance:

Strained quantum-well lasers using InGaAs and InGaAsP have been extensively used in high-speed telecommunications systems. Distributed-feedback lasers offer the advantage of a stable single longitudinal mode, enabling them to use more of the bandwidth of optical fibers than other semiconductor lasers for high-speed optical communication. This research allows us to characterize crucial parameters such as the material gain and the linewidth enhancement factor which is a fundamental measure of the chirp which limits the high-speed operation of such lasers. Our systematic experimental approach coupled with careful theoretical modeling enable us to design, fabricate, and test superior high-speed quantum-well lasers for optical communication.

6. Listing of Publications (Attached in Appendix):

i) Journal papers:

1. C. S. Chang, S. L. Chuang, J. Minch, Y. K. Chen, and T. Tanbun-Ek, "Amplified spontaneous emission spectroscopy in strained quantum-well lasers," *IEEE J. Selected*

Topics Quantum Electron., Special issue on Applied Optical Diagnostics of Semiconductors vol. 1, pp. 1100-1107, 1995.

2. J. Minch, S. L. Chuang, C. S. Chang, W. Fang, Y. K. Chen, and T. Tanbun-Ek, "Theory and experiment on the amplified spontaneous emission from distributed-feedback lasers," *Journal of Quantum Electronics* (submitted).

ii) Presentations:

3. S. L. Chuang, C. S. Chang, J. Minch, and W. Fang, "Modeling of strained quantum-well lasers and comparison with experiments," *International Symposium on Compound Semiconductors*, Cheju Island, Korea, August 28 - September 2, 1995. (Invited Talk)

4. J. Minch, C. S. Chang, W. Fang, S. L. Chuang, Y. K. Chen, and T. Tanbun-Ek, "Theory and experiment on the amplified spontaneous emission from DFB lasers," *Conference on Lasers and Electro-Optics*, Anaheim, CA, June 2-7, 1996.

5. W. Fang, C. G. Bethea, Y. K. Chen, T. Tanbun-Ek, and S. L. Chuang, "Measurement of spatially dependent carrier lifetimes in 1.55-μm DFB quantum well lasers using microwave modulation," *Conference on Lasers and Electro-optics*, Anaheim, CA, June 2-7, 1996.

7. Participants:

Faculty:	S. L. Chuang
Graduate Students:	W. Fang (1993), J. Minch (1993-1996), and T. Keating (1996)

ATTACHMENTS

Theory and Experiment on the Amplified Spontaneous Emission From Distributed-Feedback Lasers

J. Minch, S. L. Chuang, C. S. Chang, W. Fang
Y. K. Chen and T. Tanbun-Ek

This work done at the University of Illinois was supported by the U.S. Office of Naval Research under Grant N00014-96-1-0303. J. Minch was also supported by ONR AASERT Grant N00014-93-1-0844. W. Fang was supported by the AT&T Foundation Fellowship.

J. Minch, S. L. Chuang, C. S. Chang, and W. Fang are with the University of Illinois at Urbana-Champaign, Department of Electrical and Computer Engineering, 1406 W. Green Street, Urbana, IL 61801.

Y. K. Chen and T. Tanbun-Ek are with Lucent Technologies, 600 Mountain Ave., Murray Hill, NJ 07974.

Abstract

The amplified spontaneous emission of a strained quantum-well distributed feedback laser biased below laser threshold is used to extract the gain and refractive index spectra in a systematic manner. A modified Hakki-Paoli method is used to obtain the gain and differential gain spectra. The refractive index change due to carrier injection is obtained from the shift of the Fabry-Perot peaks in the amplified spontaneous emission spectrum. The measured amplified spontaneous emission spectrum, gain, refractive index change, and linewidth enhancement factor are then compared with our theoretical model for strained quantum-well lasers. Our model takes into account the realistic band structure and uses the material and quantum-well dimensions directly in the calculation of the electronic and optical properties. The theory agrees quite well with the experiment.

I. Introduction

Distributed-Feedback (DFB) lasers have become the source of choice for long distance fiber-optic telecommunication systems due to their capability for dynamic single-mode operation and their inherent temperature stability. Strained quantum-well systems have also emerged as an important technology. Producing a reduction in the hole effective mass, these lasers provide a lower threshold, higher differential gain, and lower linewidth enhancement factor. Strained quantum-well semiconductors also provide an extra degree of freedom in band-gap engineering in the search for high performance high-speed laser systems.

It is very important to be able to characterize strained quantum-well distributed-feedback lasers to both verify the physical models, and to evaluate device design. The amplified spontaneous emission (ASE) spectrum of a laser

biased below laser threshold is rich with information and particularly well suited for device characterization. Much work has been done using the ASE spectrum from Fabry-Perot lasers to measure important material parameters such as gain, differential gain, carrier-induced index shift and the linewidth enhancement factor [1],[2]. In this paper, we explore the properties of the ASE spectrum from a distributed feedback laser, developing a systematic procedure to extract these same parameters.

Previously, Soda and Imai [3] examined the spectrum by calculating the light due to a single spontaneous source exiting one of the facets (by a multiple reflection analysis using coupled-mode theory) and numerically integrating the result over the entire cavity. Makino and Glinski [4] applied transfer matrices to the same methodology to obtain an analytical expression for the spectrum. Weber and Wang [5] used an eigenmode approach to obtain an analytical result. Also, the ASE from a distributed-feedback laser has been previously used in a limited way to extract laser parameters [6] such as coupling coefficient, and gain and refractive index in the stop band region by fitting the ASE spectrum in this region. Using our model for the ASE from a distributed-feedback laser in combination with a first principles theoretical model for the electronic and optical properties of strained quantum-wells, we present a systematic method to extract the gain, refractive index change, and linewidth enhancement factor spectra from the ASE spectrum. There has been relatively little work on comparing the measured gain spectrum directly with that calculated using a realistic semiconductor quantum-well band structure. We show that the theoretical model agrees quite well with our experimental observation.

In Section II, we present our derivation for the ASE from a distributed-feedback laser, treating the spontaneous emission as current sources distributed throughout the laser cavity and solving for the electromagnetic fields in the presence of these sources. We use a comprehensive theoretical model for the gain and refractive index spectra of strained InGaAsP quantum-well lasers, designed for applications in long-wavelength 1.55 μm communication systems. Experimental procedures are discussed in Section III and methods to extract the gain based on the Hakki-Paoli method [2], refractive index change, and linewidth enhancement factor are presented in Section IV along with comparisons to theoretical calculations. Finally a brief conclusion is given in Section V.

II. Theoretical Model

A. Amplified Spontaneous Emission from a DFB laser

To derive the amplified spontaneous emission from a distributed-feedback laser, we model the spontaneous emission from a differential slice of the cavity as an effective source for optical waves. Consider an equivalent current-sheet source located at $z = z_s$, radiating in a periodic structure with gain (i.e. a DFB cavity) pictured in Fig. 1. The power radiating from this current source will be equal to the power of the spontaneous emission events occurring between z_s and $z_s + dz_s$ which couple to the lasing mode when [1]

$$|J_s| = \frac{8}{\eta} W(\hbar\omega) dz_s = \frac{4\beta}{\eta} r_{sp}(\hbar\omega) \Delta E \hbar\omega dz_s \qquad (1)$$

where β is the fraction of the spontaneous emission events which couple into the waveguide mode, $r_{sp}(\hbar\omega)\Delta E$ is the spontaneous emission rate per unit volume of

photons with energy between $\hbar\omega$ and $\hbar\omega + \Delta E$. A physical model for $r_{sp}(\hbar\omega)$ will be shown in Section II.B.

As is well known in the literature, the propagation of waves in a periodic media with a permittivity

$$\varepsilon(x,y,z) = \bar{\varepsilon}(x) + \Delta\varepsilon(x,z) \tag{2}$$

where $\bar{\varepsilon}(x)$ accounts for the index-guided single-mode waveguide with an unperturbed modal field $E_y(x)$ and $\Delta\varepsilon(x,z)$ is periodic in z, can be described by an electric field of the form

$$E = \hat{y}E_y(x)\left[A(z)e^{i\beta_o z} + B(z)e^{-i\beta_o z}\right] \tag{3}$$

where $\beta_o = \pi\ell/\Lambda$ is the Bragg wave vector, ℓ is the order of the grating, and Λ is the period of $\Delta\varepsilon$. The amplitudes A(z) and B(z) of the forward and backward propagating waves are governed by the coupled-mode equations [7], [8]

$$\frac{dA(z)}{dz} = i\Delta\beta A(z) + i\kappa_{ab}B(z) \tag{4}$$

$$\frac{dB(z)}{dz} = i\kappa_{ba}A(z) + i\Delta\beta B(z) \tag{5}$$

where $\Delta\beta = \beta - \beta_o$ is the detuning from the Bragg wavelength, β is the wavevector in the semiconductor given by $k_o n_{eff} - iG/2$ with k_o representing the wavevector in free space, n_{eff} as the effective index of the waveguide mode, and G as the modal gain, and κ_{ab} and κ_{ba} are the coupling coefficients [7].

The general solutions of the coupled-mode equations are given as

$$A(z) = Ae^{iqz} + r_m Be^{-iqz} \tag{6}$$

$$B(z) = r_p Ae^{iqz} + Be^{-iqz} \tag{7}$$

where

$$r_m = \frac{q - \Delta\beta}{\kappa_{ab}} = \frac{-\kappa_{ab}}{q + \Delta\beta} \tag{8}$$

$$r_p = \frac{q - \Delta\beta}{\kappa_{ab}} = \frac{\kappa_{ba}}{q + \Delta\beta} \tag{9}$$

and q is the eigenvalue of the coupled-mode equations given by

$$q = \pm\sqrt{(\Delta\beta)^2 - \kappa_{ab}\kappa_{ba}} \tag{10}$$

Notice that the choice of sign for q is automatically taken into account by including both forward and backward propagating parts in the amplitudes A(z) and B(z). In these equations, exactly the same analytical solutions are obtained if q is switched to -q.

It is important to understand the behavior of the complex wave number q since the waves in the periodic structure behave as if they propagate with q as their wave vector. That is, the real part of q corresponds to the propagation of the wave, and the imaginary part of q corresponds to the attenuation (or amplification) of the wave. Using $\beta = k_o n_e - iG/2$ and assuming lossless coupling, we obtain

$$q = \pm\sqrt{\left(\delta - i\frac{G}{2}\right)^2 - |\kappa_{ab}|^2} = q_r + iq_i \qquad (11)$$

where $\delta = k_o n_e - \beta_o$ is the deviation of the wave vector in the semiconductor from the Bragg wavevector and G is the gain coefficient.

The values of q_i and q_r are plotted for the positive root of q in (10) (q_r goes to δ when $|\delta| >> |\kappa_{ab}|$) in Fig. 2(a) for the negative gain case, Fig. 2(b) for the zero gain case, Fig. 2(c) for the low positive gain case, and Fig. 2(d) for the high positive gain case. The negative root of q may be obtained by flipping the signs of both real and imaginary parts. For the zero gain case we see that q is purely real for $|\delta| > |\kappa_{ab}|$, so the wave will propagate with no loss or gain. For $|\delta| < |\kappa_{ab}|$ the radiation wavelength is said to be in the stopband and q is purely imaginary. Thus, there is no propagation and the mode will be rejected by the periodic structure.

For the case with gain, as $|\delta| >> |\kappa_{ab}|$, q_r approaches δ and q_i approaches -G/2. If the radiation wavelength is far away from the stopband, it propagates as if it were in a normal waveguide, with no periodic perturbation of the permittivity function. If the radiation wavelength occurs in the stopband, there is now a finite, but small, value for the real part of q, so the mode is not entirely rejected. We see that gain tends to soften the effects of the stopband. In fact, if $|G| >> |\kappa_{ab}|$, then the waves will propagate as if there were no periodic part to the permittivity.

For the equivalent current sheet J_s at $z = z_s$, the optical electric fields can be written as

$$E_1 = \hat{y}E_y(x)\left[A_1(z)e^{i\beta_o z} + B_1(z)e^{-i\beta_o z}\right] \text{ for } 0 < z < z_s \tag{12}$$

$$E_2 = \hat{y}E_y(x)\left[A_2(z)e^{i\beta_o z} + B_2(z)e^{-i\beta_o z}\right] \text{ for } z_s < z < L \tag{13}$$

Where $A_i(z)$ and $B_i(z)$ are given by (6) and (7), with constant coefficients A_i and B_i. By matching boundary conditions at the facets, positioned at z=0 and z=L ($A_1(0) = r_1 B_1(0)$ and $B_2(L) = r_2 e^{2i\beta_o L} A_2(L)$ where r_1 and r_2 are the complex reflection coefficients), we obtain

$$\frac{A_1}{B_1} = \frac{r_1 - r_m}{1 - r_1 r_p} = c_1 \tag{14}$$

$$\frac{B_2}{A_2} = \frac{r_2 e^{2i\beta_o L} - r_p}{1 - r_2 e^{2i\beta_o L} r_m} e^{2iqL} = c_2 e^{2iqL} \tag{15}$$

The quantity c_1 (c_2) represents the total coupling of the backward (forward) to the forward (backward) propagating mode. These expressions contain the information of how the feedback from the facets, which is relatively independent of wavelength, and the feedback from the grating, which is strongly dependent on wavelength, combine to give the total coupling of the modes. c_1 and c_2 can be interpreted as the effective facet reflectivities including the effect of the grating. Whether these feedback mechanisms add constructively or destructively depends strongly on the magnitude and phase of the reflectivities of the facets.

Next, matching the boundary conditions for the tangential electric and magnetic fields at $z = z_s$, we obtain

$$A_2 = \frac{\omega\mu}{2} \frac{(c_1 a + b) J_s}{(1 - r_m r_p)\left[\beta + \frac{1}{2}\left(\kappa_{ba} e^{-2i\beta_o z_s} + \kappa_{ab} e^{2i\beta_o z_s}\right)\right](1 - c_1 c_2 e^{2iqL})} \tag{16}$$

where

$$a = \left(e^{i\beta_o z_s} + r_p e^{-i\beta_o z_s}\right) e^{iqz_s} \tag{17}$$

$$b = \left(e^{-i\beta_o z_s} + r_m e^{i\beta_o z_s}\right) e^{-iqz_s} \tag{18}$$

The transmitted electric field from the right facet is

$$E_{t2} = t_2 e^{iqL}\left(1 + c_2 r_m\right) A_2 \tag{19}$$

where t_2 is the field transmission coefficient at facet 2.

The power due to a single equivalent emission source can be integrated over the length of the cavity to obtain the total amplified spontaneous power, since the radiation from each source is incoherent. Combining (16) and (19) and ignoring the z_s dependence in the denominator (since $|\beta| >> |\kappa_{ab}|, |\kappa_{ba}|$), we obtain the total amplified spontaneous power

$$P_2 = \int_0^L \frac{|E_{t2}|^2}{2\eta_o} dz_s = \frac{(\omega\mu)^2}{8\eta_o|\beta|^2} \frac{|J_s|^2 |t_2|^2 e^{-2q_i L}}{\left|1 - r_2 e^{2i\beta_o L} r_m\right|^2 \left|1 - c_1 c_2 e^{2iqL}\right|^2} \int_0^L |c_1 a + b|^2 dz_s \tag{20}$$

This integral has several terms, but only those which are exponential or those which oscillate on the order of q_r will be significant. The final expression for the amplified spontaneous power out of the right facet is

$$P_2 = \frac{(\omega\mu)^2}{8\eta\eta_o|\beta|^2}\frac{W(\hbar\omega)|t_2|^2}{\left|1-r_2e^{2i\beta_o L}r_m\right|^2\left|1-c_1c_2e^{2iqL}\right|^2}\times$$
$$\left\{\left[\left(1+|r_m|^2\right)+|c_1|^2\left(1+|r_p|^2\right)e^{-2q_iL}\right]\left(\frac{e^{-2q_iL}-1}{-2q_i}\right)+c_1\left(r_p+r_m^*\right)e^{-2q_iL}\left(\frac{e^{2iq_rL}-1}{2iq_r}\right)+c.c.\right\} \quad (21)$$

A similar derivation can be followed to obtain the amplified spontaneous power out of facet 1.

The amplified spontaneous emission spectrum is dominated by the fast varying term $1-c_1c_2e^{2iqL}$ in the denominator of (21). The spectrum shows rapid oscillations with maximum and minimum profiles which are determined by the gain and the cavity reflection coefficients. By setting the term $\exp\left[i\left(2q_rL+\theta_{c_1}+\theta_{c_2}\right)\right]$, where θ_{c_1} and θ_{c_2} are the phases of c_1 and c_2, equal to 1 and -1 respectively, we can generate the maximum and minimum profiles. The ratio of the two is given to be:

$$S=\left(\frac{I_{\max}}{I_{\min}}\right)^{\frac{1}{2}}=\frac{1+|c_1c_2|e^{-2q_iL}}{1-|c_1c_2|e^{-2q_iL}} \quad (22)$$

This ratio is analogous to that obtained in the Hakki-Paoli method for a Fabry-Perot cavity, but here the facet reflectivities r_1 and r_2 have been replaced by c_1 and c_2, the combined reflectivity of the grating and the facets. Also, the imaginary part of the q has replaced the modal gain of the laser. This ratio will be used in section III to obtain the gain spectrum. Also, the position of the maxima are given by the formula:

$$2q_rL+\theta_{c_1}+\theta_{c_2}=2m\pi \quad (23)$$

For wavelengths away from the stopband region, $\theta_{c_1} = \theta_{r_1}$, $\theta_{c_2} = \theta_{r_2}$, and q_r becomes $k_o n_{eff}$ and the positions of the maxima reduce to the familiar formula for Fabry-Perot modes:

$$\lambda_m = \frac{2n_{eff}L}{m - \frac{\theta_{r_1}}{2\pi} - \frac{\theta_{r_2}}{2\pi}} \tag{24}$$

These mode positions will be used in section III to extract the cavity length, the effective index, and the carrier induced change in the effective index. Near the stopband, the mode positions deviate from the normal Fabry-Perot positions, so information in this area must be interpolated from the surrounding data.

B. Optical Gain and Refractive Index Model

The electronic subbands and corresponding wave functions of the strained quantum-well structure in the active region are modeled based on the effective-mass theory [9], using the theory of Bir-Pikus [10] to take into account the effects of strain. The effective-mass equation is then solved by a finite difference method [11]. The spontaneous emission rate $r_{sp}(\hbar\omega)$ for a single quantum-well can be calculated as

$$r_{sp}(\hbar\omega) = \frac{n_{eff}^2\omega^2}{\pi^2\hbar c^2}\frac{\left(2g_{sp}^{TE} + g_{sp}^{TM}\right)}{3} \tag{25}$$

$$g_{sp}^{p}(\hbar\omega) = \frac{q^2\pi}{n_{eff}c\varepsilon_o m_o^2\omega L_z}\sum_{n,m}\int\left|M_{nm}^{p}(k_t)\right|^2\frac{f_n^c(k_t)\left(1-f_n^v(k_t)\right)(\gamma/\pi)}{\left(E_{nm}^{cv}(k_t)-\hbar\omega\right)^2+\gamma^2}\frac{k_t dk_t}{2\pi} \tag{26}$$

where q is the magnitude of the electronic charge, $\hbar$ is Planck's constant divided by 2π, c is the speed of light in free space, m_o is the electron rest mass, L_z is the well width, γ is the Lorentzian half-linewidth, $f_n^c\left(f_m^v\right)$ is the Fermi occupation probability for electrons in the n^{th} (m^{th}) conduction (valence) subband, and E_{nm}^{cv} is the transition energy between the n^{th} conduction and m^{th} valence subbands. The details of the theory can be found in [1]

The material gain can be determined from the spontaneous emission rate [13] using

$$g^p = g_{sp}^p\left[1-\exp\left(\frac{\hbar\omega-\Delta F}{k_BT}\right)\right] \tag{27}$$

for p = TE or TM, and the modal gain $g_M = \Gamma^p g$ is obtained by multiplying the material gain by the optical confinement factor Γ^p, which is the polarization-dependent optical confinement of the waveguide mode weighted by n_wL_z/W_{mode}, where n_w is the number of wells and W_{mode} is the effective width of the optical mode profile. The confinement factor of the waveguide mode is calculated using the effective index method with the core dimension d, which is the total thickness of the well, barrier, and spacer layers, and the refractive indices $n(\lambda)$ of the bulk InGaAsP spacer layer and the InP cladding layer [1],[16].

The induced change in the effective index due to interband transitions is given by [7], [14]

$$\delta n_{eff}^{p}(\hbar\omega) = \Gamma^{p}\frac{q^{2}\hbar^{2}}{n_{eff}m_{o}^{2}L_{z}\varepsilon_{o}}\sum_{n,m}\int\frac{k_{t}dk_{t}}{2\pi}\left|M_{nm}^{p}(k_{t})\right|^{2} \times\frac{\left(E_{nm}^{cv}(k_{t})-\hbar\omega\right)}{E_{nm}^{cv}(k_{t})\left(E_{nm}^{cv}(k_{t})+\hbar\omega\right)}\frac{\left(f_{n}^{c}(k_{t})-f_{m}^{v}(k_{t})\right)}{\left(E_{nm}^{cv}(k_{t})-\hbar\omega\right)^{2}+\gamma^{2}} \tag{28}$$

It should be pointed out that the optical confinement factor Γ^{p} for the quantum-well active layer appears in both the modal gain g_{M} and the induced effective index change δn_{eff}. The effective index n_{eff} as a function of the carrier density N can be written as $n_{eff}(N) = n_{eff}(N = 0) + \delta n_{eff}$ and usually δn_{eff} is much smaller than $n_{eff}(N = 0)$.

The linewidth enhancement factor, which determines the semiconductor laser linewidth and plays an important role in high-speed direct modulation of the laser, can then be obtained by [15]

$$\alpha_{e} = -\frac{4\pi}{\lambda}\frac{\partial\delta n_{e}/\partial N}{\partial g_{M}/\partial N} \tag{29}$$

where $\partial g_{M}/\partial N$ is the differential gain and $\partial\delta n_{eff}/\partial N$ is the incremental change in the effective index due to carrier injection. Both a large differential gain and a small $\partial\delta n_{eff}/\partial N$ can reduce the linewidth enhancement factor α_{e}. Note that the effect of the optical confinement factor Γ^{p} is canceled in (29).

III. Experiment

The laser used in our experiment is a buried heterostructure laser grown on an InP substrate. The active region consists of seven 1.6% compressively

strained $In_{1-x}Ga_xAs_yP_{1-y}$ quantum-wells with a photoluminescence (PL) wavelength of 1.5564 μm and a well width of 70 Å. The barriers are composed of lattice matched $In_{1-x}Ga_xAs_yP_{1-y}$ with a PL wavelength of 1.255 μm and a barrier width of 100 Å. The total core is 0.25 μm thick and 1.2 μm wide. The InP cladding region is doped $n=3x10^{18}$ cm^{-3} and $p=2.5x10^{18}$ cm^{-3} on top and bottom, respectively, to provide current injection. A diagram of the bandedge profile for this laser is given in Fig. 3. One facet of the laser is cleaved while the other is AR coated.

The amplified spontaneous emission (ASE) spectrum of the distributed-feedback laser was measured using a high-resolution 1.25 meter spectrometer and a liquid-nitrogen cooled germanium detector. Measurements were made with the laser biased below threshold at several injection current levels. The temperature of the laser was maintained using a thermoelectric cooler. Heating of the laser was minimal since measurements were made below threshold. Data was taken from both facets to compare the spectra from each side.

A typical measured spectrum is shown in Fig. 4 with a detail of the behavior in the vicinity of the stopband shown in Fig. 9 (a). The spectrum shows the typical behavior of a rapid oscillation corresponding to the modes of the cavity modulated to give the maximum and minimum profiles which one would find in a Fabry-Perot semiconductor laser. However, the distributed-feedback structure introduces a well known stopband into the spectrum and enhances the modes in that vicinity, leading to possible single mode operation. The asymmetry in the spectrum around the stopband can be attributed to the feedback from the facet reflections in the DFB laser. The details of this spectrum will be discussed in the next section.

IV. Comparison Between Theory and Experiment

A. Extraction of Effective Index and Cavity Length

In order to obtain the gain coefficient and fit the ASE spectrum it is necessary to accurately obtain the cavity length and the effective refractive index of the fundamental waveguide mode. Consider two modes at λ_1 and λ_2 that are far away from the stopband with effective indices n_{eff1} and n_{eff2}, respectively. The cavity length can be solved for by using (23) evaluated at these peak wavelengths; the resulting expression is

$$L = \frac{\Delta m}{2\left(\frac{n_{eff}(\lambda_1)}{\lambda_1} - \frac{n_{eff}(\lambda_2)}{\lambda_2}\right)} \tag{30}$$

where $\Delta m = m_1 - m_2$ is the number of modes between the two wavelengths λ_1 and λ_2, and m_i is the mode number associated with the peak at λ_i. By using the formula from Adachi [16] for the refractive index of a quaternary InGaAsP semiconductor, we find the refractive indices for the waveguide layer and the InP cladding layers over the spectrum of interest. The effective index spectrum is then evaluated by using the effective index method to solve for the propagation constant of the fundamental waveguide mode. Choosing two wavelengths far apart from each other, we obtain a cavity length of 396 μm using Eq (30). Direct measurement of the cavity length under a microscope gives a cavity length of 405 μm with an error of 10 μm.

Once the cavity length is known, the mode number m_1, and hence the mode number for every mode in the spectrum, can be determined. These mode

numbers can be plugged back into (23) along with the peak wavelengths extracted from the ASE spectrum to obtain the effective index evaluated at each mode. The extracted effective index is shown in Fig. 5 as circles. The solid line is the effective index calculated using the effective index method on the laser waveguide. This fit of the effective index spectrum serves as a self-consistent check of our methodology.

B. Extraction of Gain

The modal gain spectrum of this laser is extracted using the Hakki-Paoli [2] method. If (22) is solved for the negative of the imaginary part of q, which serves as the effective gain coefficient, we obtain

$$-2q_i = \frac{1}{L}\ln\left(\frac{S-1}{S+1}\right) - \frac{1}{L}\ln\left(|c_1 c_2|\right) \tag{31}$$

The maximum and minimum profiles of the ASE spectrum were extracted and fit with a smooth curve so that the ratio between maxima and minima could be obtained using the same wavelength for each. This Hakki-Paoli ratio term (the first term on the right-hand side of Eq (31)) has a large deviation from the true gain within 25 nm of the Bragg wavelength (see Figs. 6 and 7). The deviation can be mainly attributed to the mirror loss of the cavity. The effective mirror loss term, $-\frac{1}{L}\ln|c_1 c_2|$, in (31) is the total mirror loss of the DFB cavity including the contributions of the feedback from the DFB grating and the feedback from the facets. It is convenient to break this total effective mirror loss into a mirror loss due to the facets and a mirror loss due to the DFB grating. This is done by

introducing effective DFB mirror reflectivities $b_1 = c_1/r1$ and $b_2 = c_2/r_2$ and (31) becomes

$$\begin{aligned} -2q_i &= \frac{1}{L}\ln\left(\frac{S-1}{S+1}\right) - \frac{1}{L}\ln\left(|r_1 r_2|\right) - \frac{1}{L}\ln\left(|b_1 b_2|\right) \\ &= \frac{1}{L}\ln\left(\frac{S-1}{S+1}\right) + \alpha_{FP} + \alpha_{DFB} \end{aligned} \tag{32}$$

where α_{FP} is the mirror loss of the end reflectors and α_{DFB} is the mirror loss of the DFB grating. The Fabry-Perot mirror loss term is essentially a constant over the range of interest, but the DFB mirror loss term has a dramatic dependence on wavelength, which is what ultimately leads to the selection of a single mode in the lasing spectrum, near the stopband region. This term is unknown, so we cannot obtain the true gain spectrum in this region. Away from the stopband this term vanishes, leaving the gain spectrum unpeturbed as seen in Figs. 6 and 7. We take advantage of this fact by fitting the gain data with the theory and then taking the difference between the data and the theory to estimate the effective DFB mirror loss term.

To fit the gain we use the band structure and gain theory presented in Section II. The bandgap offsets are determined from the model-solid theory [17]. When applying the theory, we assume that the quaternary $In_{1-x}Ga_xAs_yP_{1-y}$ can be linearly interpolated between InP and a ternary compound. We use $In_{1-x}Ga_xAs_yP_{1-y}$ = (1-x)InP+ x $GaAs_{y/x}P_{1-y/x}$ for x > y and $In_{1-x}Ga_xAs_yP_{1-y}$ = (1-y)InP + y $In_{1-x/y}Ga_{x/y}As$ for x < y. The material parameters used in our calculations are summarized in Table I and Table II. The bandgap offsets without the strain deformation potentials for the laser tested are found to be 303.9 meV for the conduction band and 37.1 meV for the valence band. The

bandgap renormalization is taken into account by adding $\Delta E_g^{BGR} = -CN^{1/3}$, where C is a fitting parameter [18], to the bulk bandgap E_g listed in Table I.

To match the gain data with the theory, it is necessary to accurately locate the transparency energy from the measured gain spectrum. This task is complicated since it is difficult to estimate the level of net gain at which the gain spectrum approaches a constant far below the band edge in the long wavelength limit. A solution to this problem is to measure the gain for both TE and TM polarizations from the laser since both spectra must cross the transparency level at F_c-F_v, the quasi-Fermi level separation energy. Fig. 6 shows the experimental data for $\frac{1}{L}\ln\left[\frac{S-1}{S+1}\right]$ measured at 20°C for TE and TM polarizations at injection currents of 2.5 and 3.5 mA. This data was measured at a temperature lower than the data to be matched in an effort to shift the transparency energies away from the stopband regions where the effective DFB mirror loss can shift the crossing point away from the transparency level. The temperature can cause this level to shift, due to the temperature dependence of the intrinsic loss, however, over this small temperature change, this shift would be negligible. From our measurement, we estimate the transparency level to be -60 cm^{-1}.

In Fig. 7 we show the measured and calculated TE polarized modal gain spectrum at five injection current levels at T= 30°C The carrier densities are determined by using the calculated bandstructure to find the carrier density which gives a quasi-Fermi level separation equal to the transparency energy for each of the current injection levels. Next, the value of C is varied to match the peak gain wavelength of the middle (3 mA) gain spectrum. That same value is then used to determine the final carrier densities at each of the other current injection levels. The carrier densities are found to be N = 9.6×10^{17} , 1.25×10^{18} , 1.375×10^{18} , 1.485×10^{18} , and 1.53×10^{18} cm^{-3}, for the injection currents 1, 2, 3, 4,

and 5 mA respectively. The bandgap renormalization coefficient is found to shift the bandgap by 13 meV for a two-dimensional (2D) carrier density of 1×10^{12} cm^{-2}. The experimental data and the theoretical curves agree quite well with each other. Also, the effects of bandfilling, which blue shift the peak gain wavelength and increase the bandwidth of the gain spectrum are clearly demonstrated in Fig. 7

C. *DFB Effective Mirror Loss*

We estimate the effective mirror loss of our laser by taking the difference between the Hakki-Paoli gain data and the theoretical fit of that data. Fig. 8 shows a plot of this difference with the symbols representing the difference at a current of 4 mA. The solid curve shows the theoretical effective DFB mirror loss. The magnitudes of r_1 and r_2 were chosen such that r_2 has a small reflectivity and r_1 has the reflectivity of a cleaved facet. The phases of the facet reflectivities are virtually impossible to control in practice, so they are varied to fit the full ASE spectrum. The coupling coefficient and Bragg wavelength are also treated as fitting parameters. The values used to fit the full ASE spectrum as discussed in the next section were used to produce this curve. We see that the effective DFB mirror loss explains the deviation of the Hakki-Paoli gain data from the actual gain very well. It is very important to combine both theory and experiment to extract the gain accurately especially near the stopband region because of the strong wavelength dependence of the DFB mirror loss.

D. *Fit of ASE Spectrum*

The full ASE spectrum from both facets of the laser can be fitted with our theory. Fig. 9 (a) shows the measured amplified spontaneous emission spectrum

near the stopband region from both laser facets with the laser biased just below threshold (I=4 mA , I_{th} = 4.7 mA) at a temperature of 30°C. We see for our laser that there is only a small difference between the spectra from the two facets. This difference can be explained by the fact that the forward and backward propagating waves see different structures leading to different effective transmissions for the two facets. There is no difference in the selection of modes, however. Fig. 9 (b) shows our calculated spectra using (21) with our theoretical model for the effective index spectrum and the gain spectrum, with the extracted cavity length, and facet reflectivities of $|r_1| = .55$, $\Phi_1=85°$ and $|r_2| = .27$, $\Phi_2 = 70°$, a coupling coefficient of 30 cm^{-1}, and a Bragg wavelength of 1.5521 μm. These values were used to fit the DFB mirror loss in the previous section. We see that the calculated spectra are able to match the behavior of the measured spectra very well for each facet.

E. Differential Gain, Refractive index change, and Linewidth Enhancement Factor

Measured (symbols) and calculated (solid) curves for the differential gain (dG/dI) are given in Fig. 10 at I = 2.5, 3.5 and 4.5 mA. The differential gain is obtained directly from the extracted gain data by taking the difference between two gain spectra at two nearby current levels and dividing by the current level difference (ΔI = 1 mA). We ignore the DFB mirror loss term since it is weakly dependent on gain. Inside of the stopband region, the differential gain can be interpolated from the data around it. The strong dependence in the differential gain spectra is due to the filling of the electronic bands. Carriers fill the lower energy states first and slowly fill the higher states as more and more are injected. A change in the level of carrier injection will lead to a larger change in the population at higher energies since there are more states available there and in

turn will cause the larger differential gain. At higher current injection levels, the differential gain decreases because of the same effect and also because the bands start to saturate.

The carrier-induced index shift may be obtained by studying the shift of the mode positions with current injection. Each peak wavelength demonstrates a blue shift with higher current injection and can be measured as a function of injection current. Using (23) and including the dispersion of n_{eff}, the relationship between $\lambda(I)$ and the carrier induced index shift can be derived to be:

$$\frac{\partial n_{eff}}{\partial I} = \frac{n_{eff}}{\lambda}\left(1 - \frac{\lambda}{n_{eff}}\frac{\partial n_{eff}}{\partial \lambda}\right)\frac{\partial \lambda}{\partial I} \tag{33}$$

The resulting carrier induced index shift for the laser is shown in Fig. 11 (symbols are the experimental data and solid curves are the theoretical results). The effective index shifts to smaller values as the injection current is increased. In contrast to the differential gain, the effective index change is very weakly dependent on wavelength. Also, as the injection current level is increased, the change in effective index decreases. The reason for this saturation effect is similar to what happens to the differential gain as explained above. Again data in the stopband can be interpolated from the surrounding data outside of the stopband.

The linewidth enhancement factor is obtained from the ratio between the carrier induced index shift and the differential gain. Using the extracted data from above, the linewidth enhancement factor is plotted in Fig 12. The solid lines represent the theoretical plot using (29). The wavelength dependence of α_e

is almost entirely due to the wavelength dependence of the differential gain. As the current is increased, α_e increases slightly. At laser threshold (1.55 μm, and 4.7 mA), α_e is about 3.5. We can see the agreement is good for the currents at I= 2.5 and 3.5 mA. At I=4.5 mA, the errors are larger because of the smaller dG/dI, which makes the errors in α_e bigger than those at the two other currents.

V. Conclusions

We have presented a theoretical model and a systematic experimental procedure to extract the gain, refractive index and linewidth enhancement factor from the amplified spontaneous emission spectrum of an InGaAsP strained quantum-well distributed-feedback laser. The theoretical ASE spectrum has been used to match the experimental data and to extract the coupling coefficient and the facet reflectivities The measured effective index spectrum agrees well with the theoretically calculated values, and the extracted cavity length is in excellent agreement with a direct measurement. The gain spectrum can be extracted accurately using the Hakki-Paoli method by carefully accounting for the effective mirror loss of the DFB laser. Also, tracking the differential gain along with the shift of modes with injection current allows measurement of the linewidth enhancement factor, which is a crucial parameter for the high speed modulation of DFB lasers used in long-distance fiber communication systems. We also show that a first-principle calculation using the material and structural parameters of a strained quantum-well laser agrees very well with the experimental data for the optical gain and the refractive index change. Our theoretical approach and systematic experimental procedure provide an efficient and accurate tool in the design of DFB strained quantum-well semiconductor lasers.

References

[1] C. S. Chang, S. L. Chuang, J. Minch, W. Fang, Y. K. Chen, and T. Tanbun-Ek, "Amplified spontaneous emission spectroscopy in strained quantum-well lasers," *IEEE J. Selected Topics Quantum Electron.*, vol. 1, pp. 1100-1107. 1995

[2] B. W. Hakki and T. L. Paoli, "CW degradation at 300K of GaAs double-heterostructure junction lasers. II. Electronic gain," *J. Appl. Phys.*, vol. 44, pp. 4113-4119, 1973

[3] H. Soda and H. Imai, "Analysis of the spectrum behavior below the threshold in DFB lasers," *IEEE J. Quantum Electron.*, vol. QE-22, pp. 637-641, 1986.

[4] T. Makino and J. Glinkski, "Transfer matrix analysis of the amplified spontaneous emission of DFB semiconductor laser amplifiers," *IEEE J. Quantum Electron.*, vol. 24, pp. 1507-1518, 1988.

[5] J.-P. Weber and S. Wang, "New method for the calculation of the emission spectrum of DFB and DBR lasers," *IEEE J. Quantum Electron.*, vol. 27, pp. 2256-2266, 1991.

[6] R. Schatz, E. Berglind, and L. Gillner, "Parameter extraction from DFB lasers by means of a simple expression for the spontaneous emission spectrum," *IEEE Photon Technol. Lett.*, vol. 6, pp. 1182-1184, 1994.

[7] S. L. Chuang, *Physics of Optoelectronic Devices*, New York: Wiley, 1995.

[8] H. Kogelnik and C. V. Shank, "Coupled-wave theory of distributed feedback lasers," *J. Appl. Phys.*, vol. 43, pp. 2327-2335, 1972.

[9] J. M. Luttinger and W. Kohn, "Motion of electrons and holes in perturbed periodic field," *Phys. Rev.*,vol. 97, pp. 869-883, 1955.

[10] G. L. Bir and G. E. Pikus, *Symmetry andStrain-Induced Effects in Semiconductors*, John Wiley, New York, 1974.

[11] C. S. Chang and S. L. Chuang, "Modeling of strained quantum-well lasers with spin-orbit coupling," *IEEE J. Selected Topics in Quantum Electron.*, vol. 1, pp. 218-229, 1995.

[12] *Numerical Data and Functional Relationships inScience and Technology,* edited by K.-H. Hellwege, Landolt-Bornstein, New Series,Groups III-V, vol. 17a, Springer, Berlin, 1982; Groups III-V, Vol. 22a, Springer, Berlin, 1986.

[13] S. L. Chuang, J. O'Gorman, and A. F. J. Levi, "Amplified spontaneous emission and carrier pinning in laser diodes," *IEEE J. Quantum Electron.*, vol. 29, pp. 1631-1639, 1993.

[14] Y. C. Chang, J. N. Schulman, and U. Efron, "Electro-optic effect in semiconductor superlattices," *J. Appl. Phys.*, vol. 62, pp. 4533-4537, 1987.

[15] C. H. Henry, "Theory of the linewidth of semiconductor lasers," *IEEE J. Quantum Electron.*, vol. QE-18, pp. 259-264, 1982.

[16] S. Adachi, "Refractive indicies of III-V compounds: key properties of InGaAsP relevant to device design," *J. Appl. Phys.*, vol. 53, pp. 5863-5869, 1982.

[17] C. G. Van de Walle, "Band lineups and deformation potentials in the model-solid theory", *Phys. Rev. B*, vol. 39, pp. 1871-1883, 1989.

[18] G. Trankle, E. Lach, A. Forchel, F. Scholz, C. Ell, H. Haug, and G. Weimann, "General relation between bandgap renormalization and carrier density in two-dimensional electron-hole plasmas," *Phys. Rev. B*, vol. 36, pp. 6712-6714, 1987.

Figure Captions

Figure 1 - A schematic of the distributed-feedback laser cavity showing the amplified spontaneous emission from both facets. An equivalent current sheet is shown as the source of spontaneous emission at $z = z_s$. The total amplified spontaneous emission power emitted from the laser is found by integrating the resulting power from a single source over the position of the current source z_s along the length of the cavity.

Figure 2 - Plots of the real and imaginary parts of qL with (a) GL = -0.8 , (b) GL = 0, (c) GL = 0.8, and (d) GL = 2.4. $\kappa_{ab}L=\kappa_{ba}L=2$ in these plots.

Figure 3 - The conduction and valance band edge profiles of the strained InGaAsP quantum-well laser used in our experiment. The wells are compressively strained InGaAsP with a PL wavelength of 1.5564 μm. The barriers are made of lattice matched InGaAsP with a PL wavelength of 1.255 μm.

Figure 4 - The amplified spontaneous emission spectrum from a distributed-feedback laser biased below laser threshold showing the longitudinal modes and the selection of modes near the stopband region due to the periodic grating.

Figure 5 - A plot of the effective index extracted from the mode positions in Fig. 3 as a function of wavelength. The open circles are experimental data. The solid line gives the theoretically calculated effective index profile using the refractive index from [16] for the InGaAsP core layer and the InP cladding. From the theoretical fit we obtain a cavity length of 396 μm.

Figure 6 - A plot of the Hakki-Paoli ratio for TE and TM polarizations measured at 20°C. From the intersection of the TE and TM curves, we determine the transparency level to be -60 cm^{-1}.

Figure 7 - A plot of the measured TE modal gain spectra up to laser threshold at I = 1, 2, 3, 4, and 5 mA. The theoretical material gain multiplied by the optical confinement factor is also plotted (solid lines).

Figure 8 - A plot of the total effective DFB mirror loss for the laser under study (symbols). The solid line represents the theoretical effective DFB mirror loss using the same parameters as the fit of the ASE spectrum in Fig. 9.

Figure 9 - (a) A plot of the measured amplified spontaneous emission from both laser facets at 30°C and an injection current (4 mA) below laser threshold. (b) The theoretically calculated amplified spontaneous emission spectrum for both facets using the extracted effective index and gain profiles. The theory explains the behavior of the measured spectra very well.

Figure 10 - A plot of the measured differential gain (symbols) compared with our theoretical calculations (solid curves) for I = 2.5, 3.5 and 4.5 mA.

Figure 11 - A plot of the measured carrier induced effective index change (symbols) compared with our theoretical calculations (solid lines).

Figure 12 - A plot of the linewidth enhancement factor for our laser obtained from the ratio of Figs. 10 and 11 (symbols) compared to our theoretical calculations (solid curves).

TABLE I

MATERIAL PARAMETERS USED FOR THE CALCULATIONS [12]

$In_{1-x}Ga_xAs_yP_{1-y}$ well	$x = 0.09, y = 0.70$
Electron effective mass m_n/m_o	$0.08 - 0.116y + 0.026x + 0.06y^2 + 0.064x^2 - 0.059xy + 0.032xy^2 - 0.02x^2y$
Bandgap E_g (eV)	$1.35 + 0.642x - 1.101y + 0.758x^2 + 0.101y^2 - 0.159xy - 0.28x^2y + 0.109xy^2$
$In_{1-x}Ga_xAs_yP_{1-y}$ barrier	$x = \frac{0.1894y}{0.4184 - 0.013y}$
Bandgap E_g (eV)	$1.35 - 0.775y + 0.149y^2$
Electron effective mass m_n/m_o	$0.08 - 0.039y$

* The quaternary interpolation formula, $P(In_{1-x}Ga_xAs_yP_{1-y}) = xyP(GaAs)+x(1-y)P(GaP) + (1-x)yP(InAs) + (1-x)(1-y)P(InP)$ is used for the Luttinger parameters γ_1, γ_2, and γ_3, spin-orbit split-off energy Δ, and the energy parameter E_P [1]. The material parameters for GaAs, GaP, InAs, and InP are taken from [7], [12], and [17], and are listed in Table II

TABLE II
MATERIAL PARAMETERS FOR BINARY
COMPOUND SEMICONDUCTORS [7], [12], [17]

	GaAs	InAs	GaP	InP
γ_1	6.80	20.4	4.05	4.95
γ_2	1.90	8.30	0.49	1.65
γ_3	2.73	9.10	1.25	2.35
Spin-orbit energy Δ (eV)	0.34	0.38	0.08	0.11
Optical-matrix Energy parameter E_p (eV)	25.7	22.2	22.2	20.4

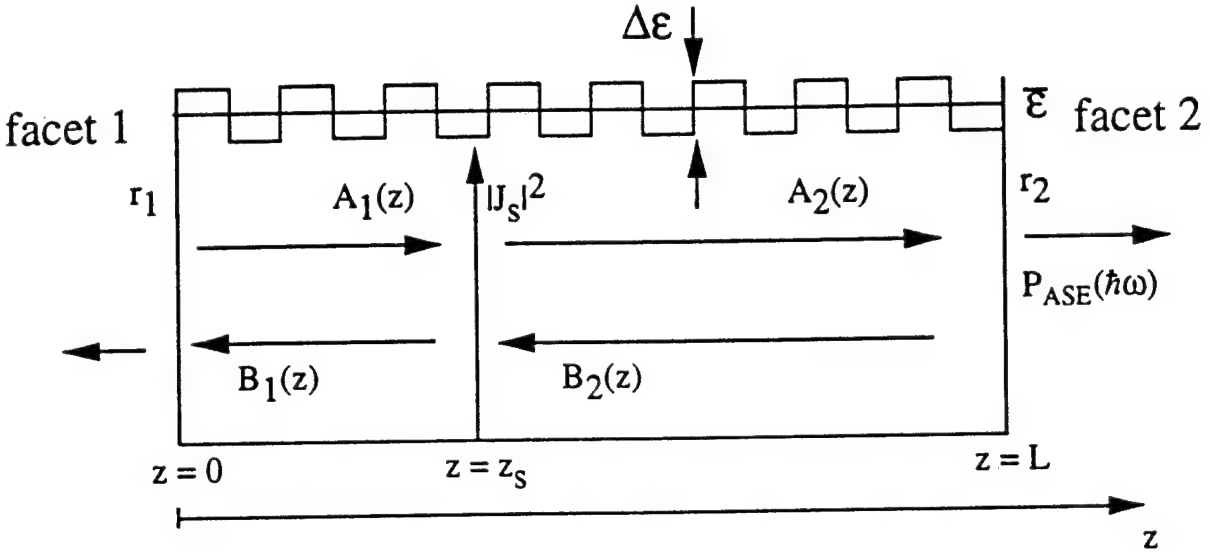

Fig. 1

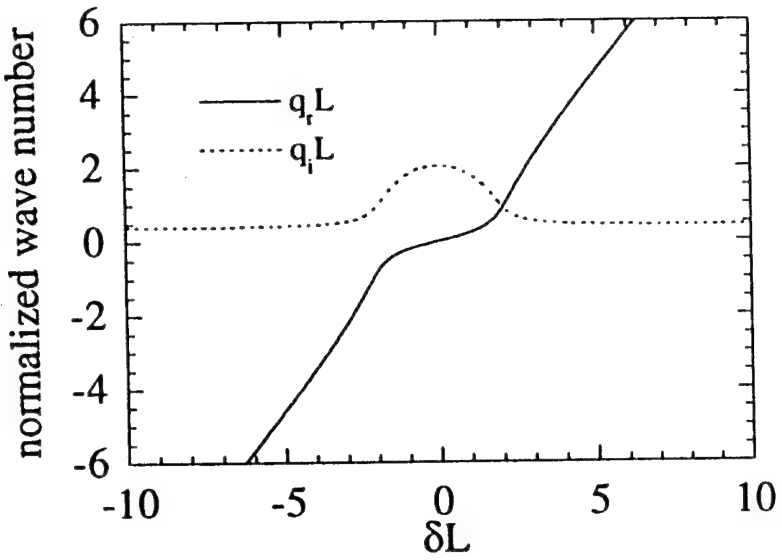
normalized wave number
6
4
2
0
-2
-4
-6
-10
-5
0
5
10
δL
q_rL
q_iL

(a)

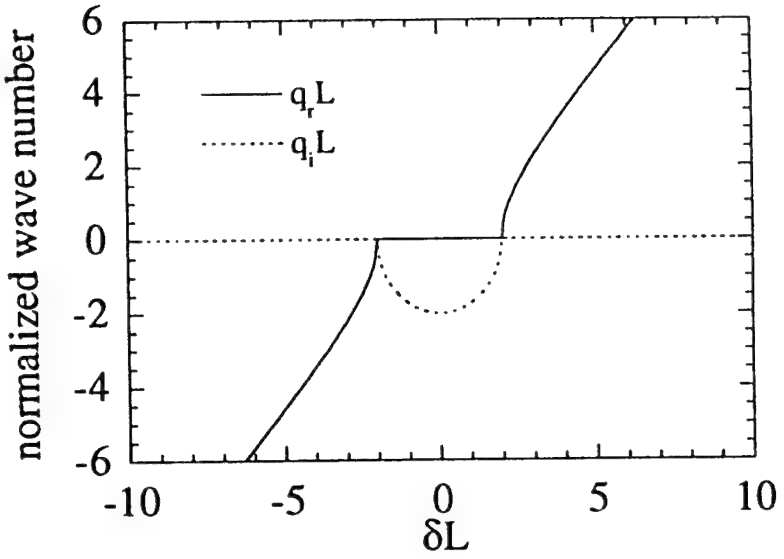
normalized wave number
6
4
2
0
-2
-4
-6
-10
-5
0
5
10
δL
q_rL
q_iL

(b)

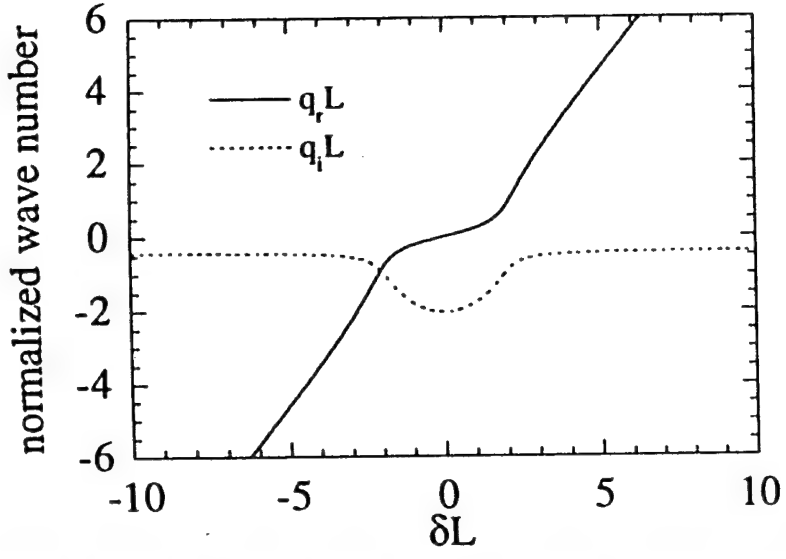
normalized wave number
6
4
2
0
-2
-4
-6
-10
-5
0
5
10
δL
q_rL
q_iL

(c)

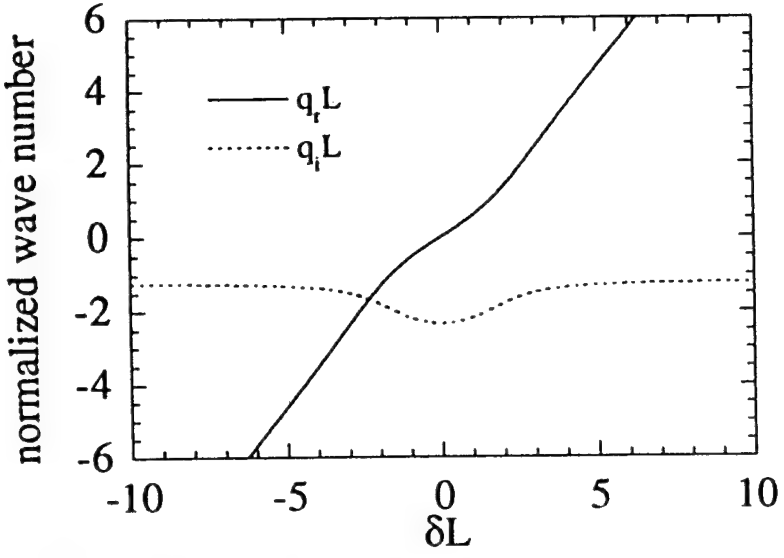
normalized wave number
6
4
2
0
-2
-4
-6
-10
-5
0
5
10
δL
q_rL
q_iL

(d)

Fig. 2

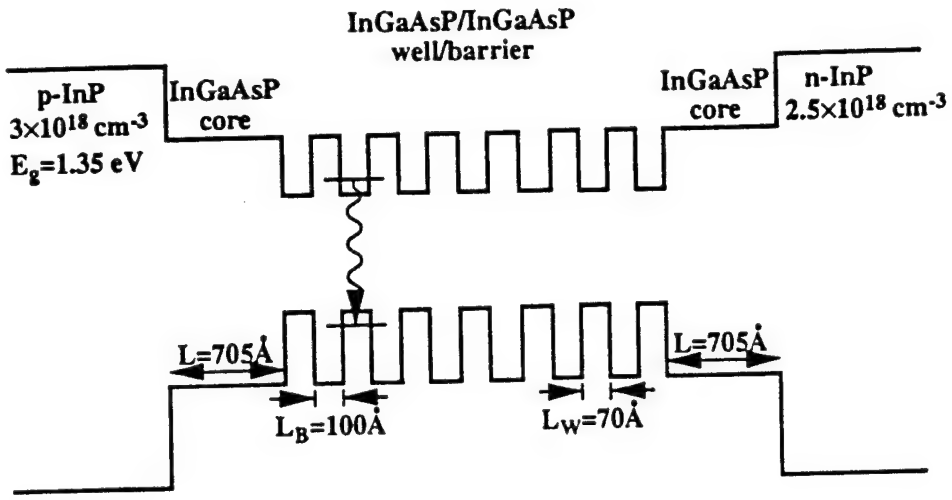
InGaAsP/InGaAsP
well/barrier
p-InP
3×10^18 cm^-3
E_g=1.35 eV
InGaAsP
core
InGaAsP
core
n-InP
2.5×10^18 cm^-3
L=705Å
L=705Å
L_B=100Å
L_W=70Å

Fig. 3

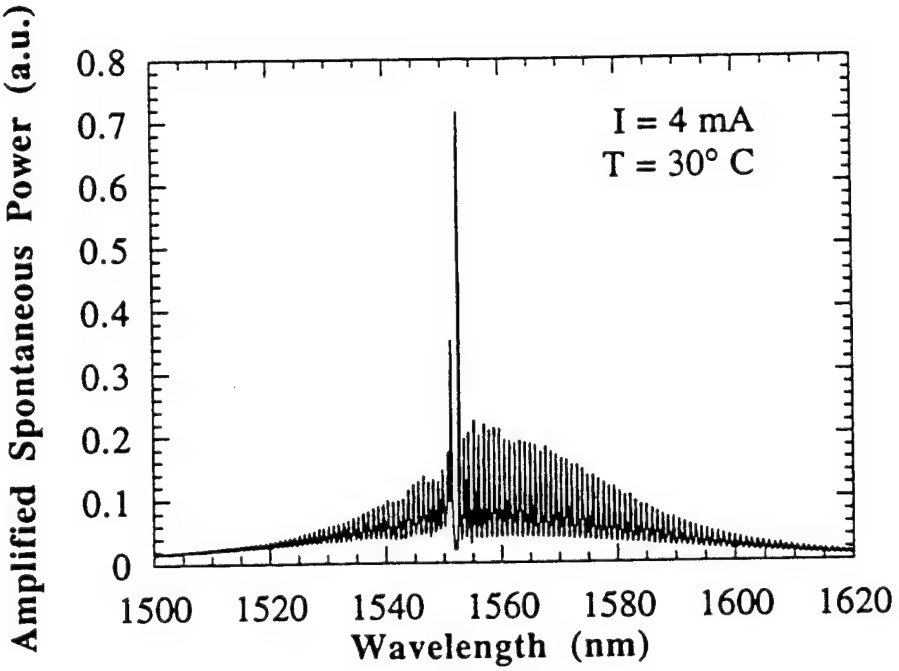
Amplified Spontaneous Power (a.u.)
0.8
0.7
0.6
0.5
0.4
0.3
0.2
0.1
0
I = 4 mA
T = 30° C
1500
1520
1540
1560
1580
1600
1620
Wavelength (nm)

Fig 4.

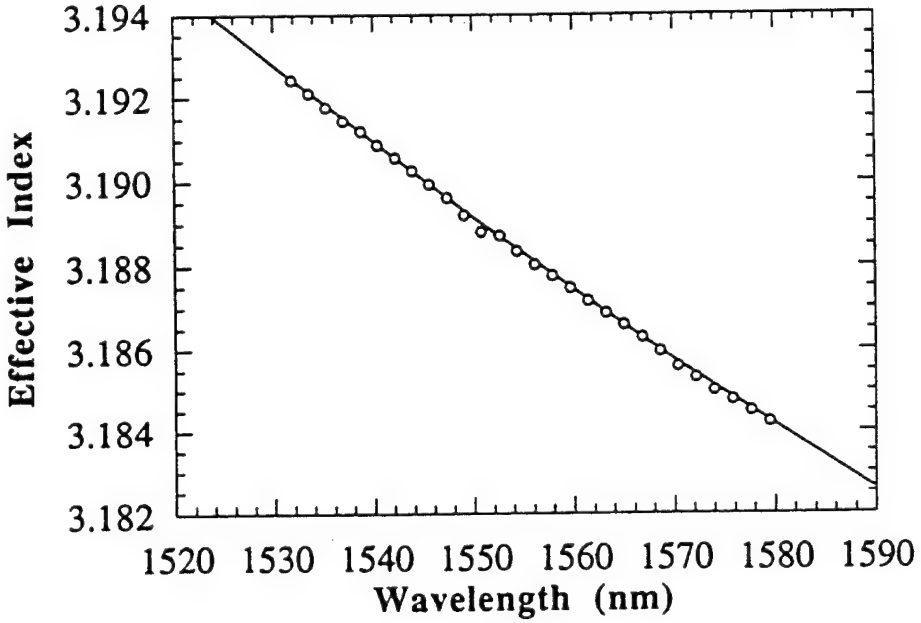
3.194
3.192
3.190
3.188
3.186
3.184
3.182
Effective Index
1520 1530 1540 1550 1560 1570 1580 1590
Wavelength (nm)

Fig. 5

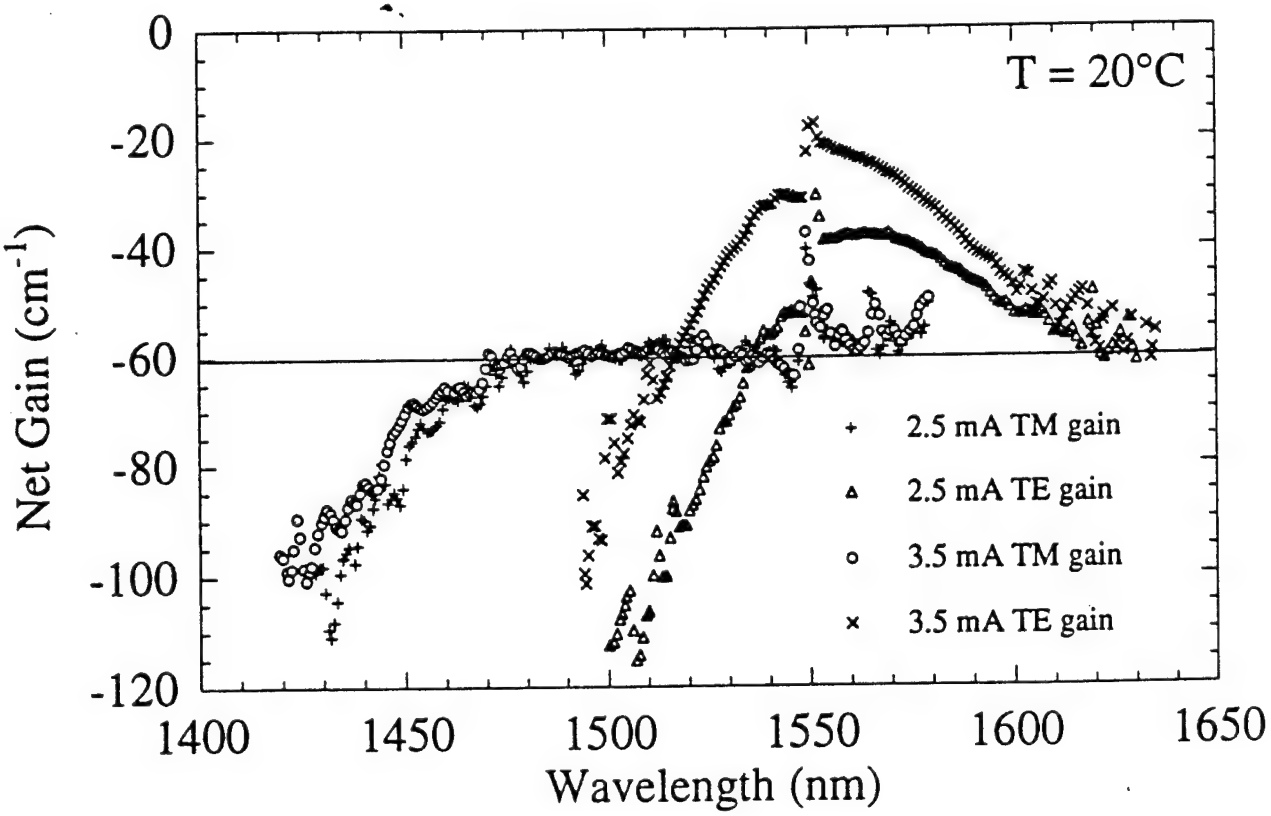
T = 20°C
2.5 mA TM gain
2.5 mA TE gain
3.5 mA TM gain
3.5 mA TE gain
Net Gain (cm-1)
Wavelength (nm)
0
-20
-40
-60
-80
-100
-120
1400
1450
1500
1550
1600
1650

Fig. 6

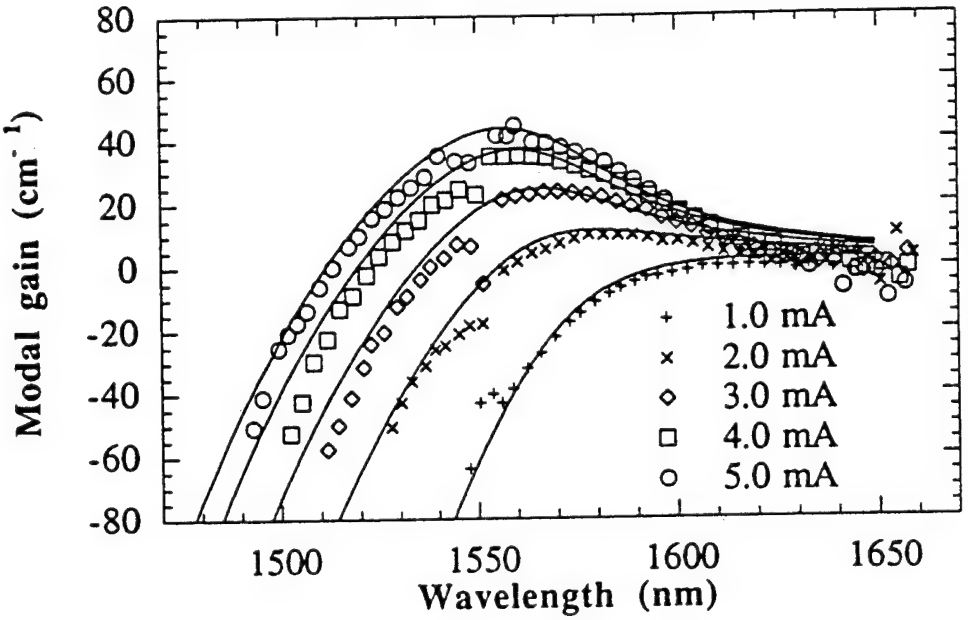
80
60
40
20
0
-20
-40
-60
-80
Modal gain (cm^{-1})
1500
1550
1600
1650
Wavelength (nm)
1.0 mA
2.0 mA
3.0 mA
4.0 mA
5.0 mA

Fig. 7

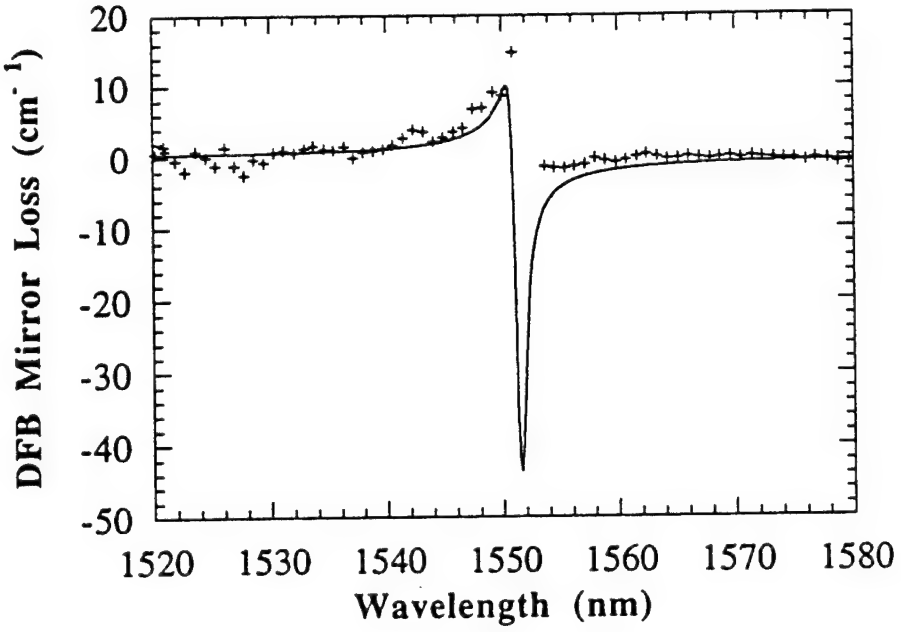
DFB Mirror Loss (cm-1)
20
10
0
-10
-20
-30
-40
-50
1520
1530
1540
1550
1560
1570
1580
Wavelength (nm)

Fig. 8

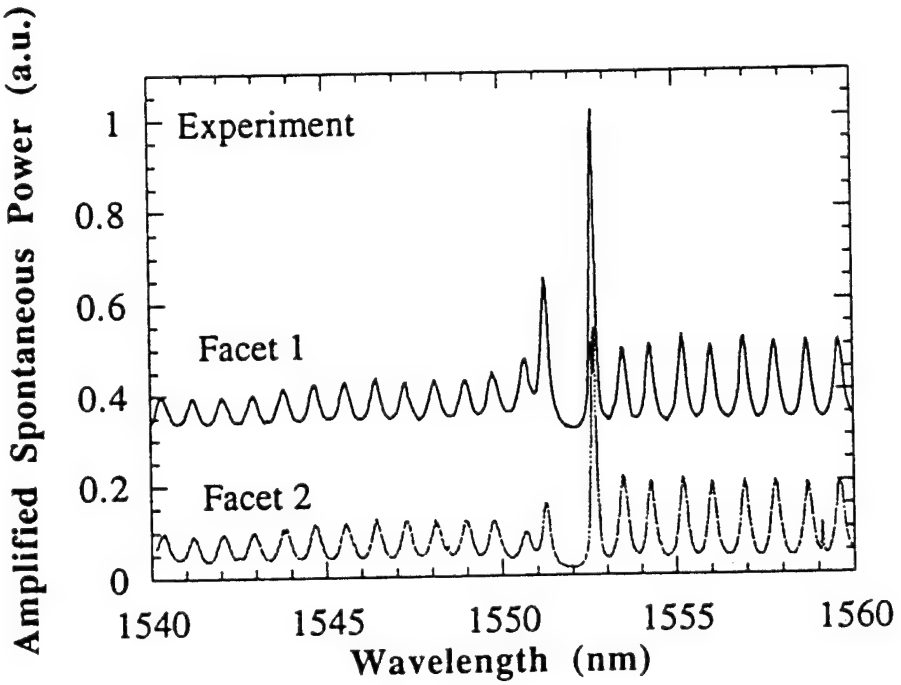
Amplified Spontaneous Power (a.u.)
1
0.8
0.6
0.4
0.2
0
Experiment
Facet 1
Facet 2
1540
1545
1550
1555
1560
Wavelength (nm)

Fig. 9 a

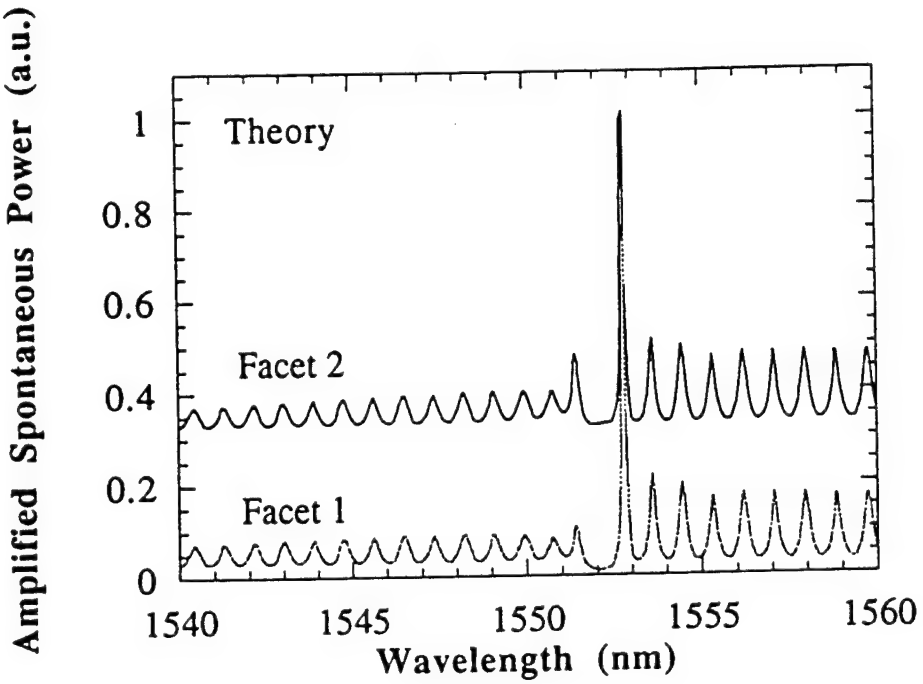
Amplified Spontaneous Power (a.u.)
1
0.8
0.6
0.4
0.2
0
Theory
Facet 2
Facet 1
1540
1545
1550
1555
1560
Wavelength (nm)

Fig. 9 b

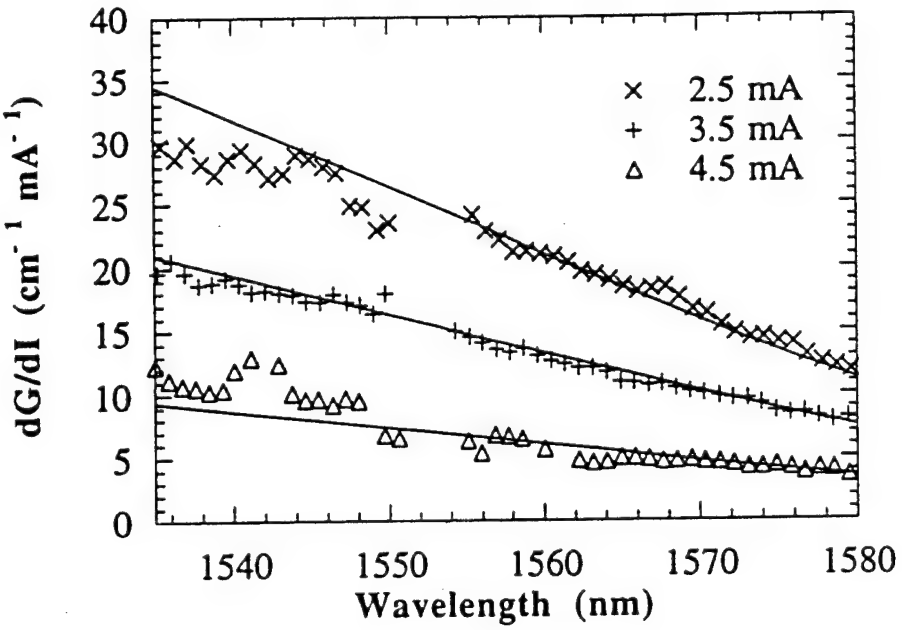
40
35
30
25
20
15
10
5
0
dG/dI (cm⁻¹ mA⁻¹)
2.5 mA
3.5 mA
4.5 mA
1540
1550
1560
1570
1580
Wavelength (nm)

Fig. 10

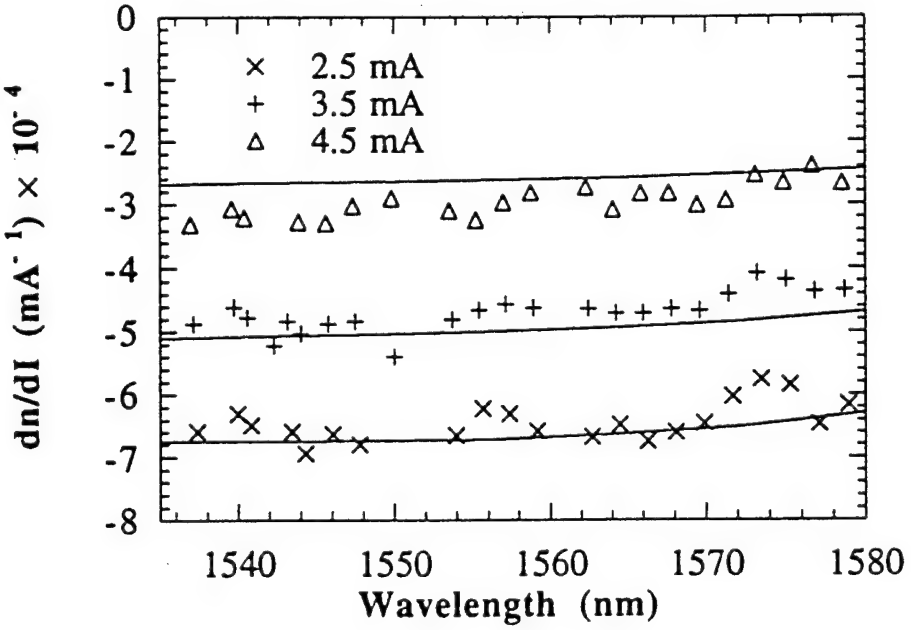
0
-1
-2
-3
-4
-5
-6
-7
-8
dn/dI (mA⁻¹) × 10⁻⁴
2.5 mA
3.5 mA
4.5 mA
1540
1550
1560
1570
1580
Wavelength (nm)

Fig. 11

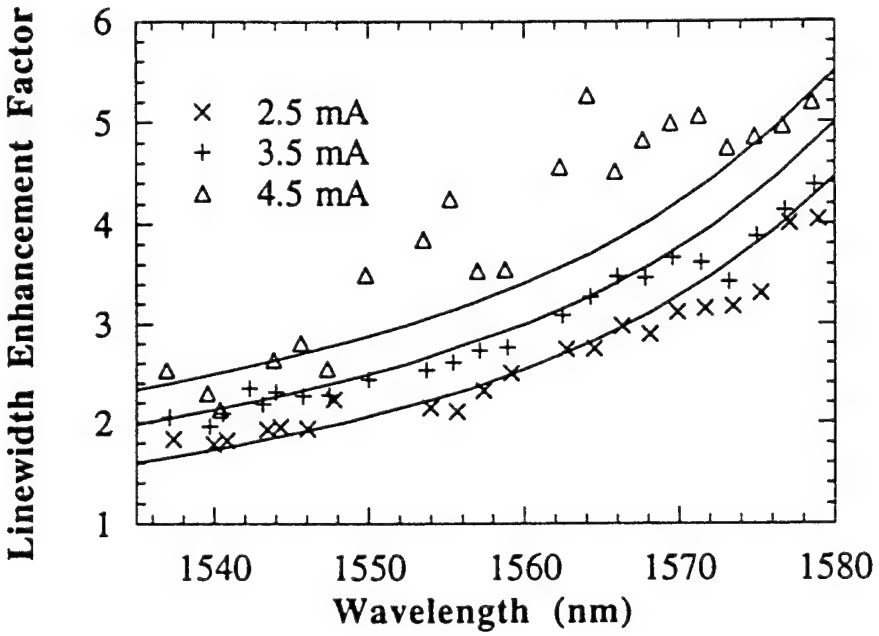
Linewidth Enhancement Factor
6
5
4
3
2
1
2.5 mA
3.5 mA
4.5 mA
1540
1550
1560
1570
1580
Wavelength (nm)

Fig. 12

Inst. Phys. Conf. Ser. No 145: Chapter 10
Paper presented at 22nd Int. Symp. Compound Semiconductors, Cheju Island, Korea, 28 August–2 September 1995

Modeling of strained quantum-well lasers and comparison with experiments

S L Chuang[1], C S Chang, J Minch and W Fang

University of Illinois at Urbana-Champaign
Department of Electrical and Computer Engineering
1406 W. Green Street, Urbana, Illinois 61801, U. S. A.

Abstract. We discuss a general theory for strained quantum-well lasers starting from an expression for amplified spontaneous emission. The electronic band structure, optical gain spectrum, refractive index change and the linewidth enhancement factor in the presence of carrier injection are calculated by taking into account the valence band-mixing effects. We show that our theoretical results compare very well with experimental data for strained InGaAsP quantum-well lasers obtained by measuring the amplified spontaneous emission spectrum as a function of the injection current.

1. Introduction

Strained quantum-well lasers have been of great interest in many semiconductor material systems covering from visible to near-infrared regions of the spectrum. The modeling of strained quantum-well lasers [1, 2, 3] poses a challenging task because many important material parameters for the electronic properties such as the effective masses, the band edge discontinuity ratio, and the deformation potentials in strained ternary and quaternary quantum-well systems have not been well documented or experimentally determined. Very often, a linear interpolation scheme from the binary compound semiconductors has to be adopted. Optical properties such as the refractive index and the optical gain coefficient as a function of the injection current in a semiconductor laser have to be determined taking into account the optical waveguide effects in a realistic quantum-well laser structure using double confinement. To date, little work has been done to compare directly theoretical results with experimental data obtained for the optical gain spectrum and the induced change in refractive index in a population inverted medium using strained quantum wells.

We have developed a comprehensive theoretical model [1, 3] including the valence-band mixing effects for strained InGaAsP quantum-well lasers. The optical gain coefficient and the refractive index change as a function of the injection carrier density were

[1] E-mail: s-chuang@uxh.cso.uiuc.edu, Phone: 1-217-333-3359, Fax: 1-217-333-5701

calculated first, taking into account band gap renormalization. Then the linewidth enhancement factor [4], which determines the laser spectral linewidth and also affects the laser chirps in high-speed modulation, was calculated. We next measured the amplified spontaneous emission spectrum from an index-guided InGaAsP quantum-well laser as a function of the injection current. The optical gain spectrum, refractive index profile and the linewidth enhancement factor were obtained directly from the amplified spontaneous spectra at different injection currents. By taking into account the dispersion effects of the refractive index in calculating the optical confinement factor and the modal gain, our theoretical results agree very well with the experimental data.

2. Theory

2.1. Amplified spontaneous emission spectroscopy

The amplified spontaneous emission is modeled as a distribution of uniform electromagnetic (optical) current sheet along the longitudinal direction z. The magnitude of the current sheet is chosen to have a radiation power density to the right $W(\hbar\omega)$ (W/cm^3) equal to half of the spontaneous emission power density that coupled into the waveguide mode,

$$W(\hbar\omega) = \frac{\beta}{2} r_{sp}(\hbar\omega)\Delta E\,\hbar\omega \tag{1}$$

where β is the fraction of the spontaneous emission events that are coupled into the waveguide mode, and $r_{sp}(\hbar\omega)\Delta E$ is the spontaneous emission rate per unit voulme of photons with energy between $\hbar\omega$ and $\hbar\omega + \Delta E$.

The fields due to the current sheet at $z = z_s$ can be written as superpositions of a forward and a backward propagating wave inside and outside the cavity. By matching the boundary conditions for the tangential electric and magnetic fields at the two mirrors and $z = z_s$, the intensity of the output wave (light) from the right facet $I(z_s, \hbar\omega)$ can be determined. Due to the incoherent nature of the spontaneous emission events, the total amplified spontaneous emission intensity $I_{ASE}(\hbar\omega)$ can be found by integrating the intensity $I(z_s, \hbar\omega)$ over the cavity. The final expression $I_{ASE}(\hbar\omega)$ is found to be

$$I_{ASE}(\hbar\omega) = (1-R)\left(\frac{W(\hbar\omega)L}{GL}\right)\frac{(e^{GL}-1)(1+Re^{GL})}{|1-Re^{GL}e^{i2k_o n_e L}|^2} \tag{2}$$

where we have assumed both left and right mirrors have the same field reflection coefficient $\sqrt{R}$, $k_o = 2\pi/\lambda$, λ is the wavelength in free space, n_e is the effective index of the waveguide mode, L is the cavity length, $G = g_M - \alpha_i$ is the net gain, g_M is the modal gain, and α_i is the intrinsic loss.

2.2. Gain and refractive index model with valence band-mixing

The subband structures are solved by the effective mass theory [5] with a 6×6 Hamiltonian which includes the valence band mixing between the heavy-hole, light-hole, and spin-orbit split-off bands. The theory of Bir-Pikus [6, 7] is used to take into account the effects of strain. The spontaneous emission rate $r_{sp}(\hbar\omega)$ for a single quantum-well can be calculated as

$$r_{sp}(\hbar\omega) = \frac{n_e^2\omega^2}{\pi^2\hbar c^2}\left\{\frac{q^2\pi}{n_e c\epsilon_o m_o^2\omega L_z}\sum_{n,m}\int |\mathrm{M}_{nm}^{sp}(k_t)|^2\,\frac{f_n^c(k_t)\,(1-f_m^v(k_t))\,(\gamma/\pi)}{(E_{nm}^{cv}(k_t)-\hbar\omega)^2+\gamma^2}\,\frac{k_t dk_t}{2\pi}\right\} \tag{3}$$

where L_z is the well width, f_n^c (f_m^v) is the Fermi occupation probability for electrons (holes) in the n_{th} (m_{th}) conduction (valence) subband, E_{nm}^{cv} is the transition energy between the n_{th} conduction and m_{th} valence subbands, $M_{nm}^{sp} = (2M_{nm}^{TE} + M_{nm}^{TM})/3$, M_{nm}^{TE} (M_{nm}^{TM}) is the momentum matrix element for the TE (TM) polarization.

The material gain can be determined from the spontaneous emission rate using [8]

$$g^p = g_{sp}^p \left[1 - \exp\left(\frac{\hbar\omega - \Delta F}{k_B T} \right) \right] \tag{4}$$

where the superscript p stands for polarization, $p = TE$ or $p = TM$, ΔF is the seperation between the electron and hole quasi-Fermi level, and g_{sp}^p is the expression inside the curly braket of Equation (3) with M_{nm}^{sp} change to M_{nm}^p. The modal gain is obtained by multiplying the material gain by the optical confinement factor Γ for the well regions. Γ can be estimated by weighting the optical confinement factor for the waveguide mode with $n_w L_z / W_{mode}$, where n_w is the number of wells and W_{mode} is effective width of the waveguide mode.

The induced change in the effective refractive index due to interband transitions is

$$\delta n_e(\hbar\omega) = \Gamma \frac{q^2\hbar^2}{n_e m_o^2 L_z \epsilon_0} \sum_{n,m} \int \frac{k_t dk_t}{2\pi} |M_{nm}^p|^2 \frac{(E_{nm}^{cv} - \hbar\omega)}{E_{nm}^{cv}(E_{nm}^{cv} + \hbar\omega)} \frac{(f_n^c - f_m^v)}{(E_{nm}^{cv} - \hbar\omega)^2 + \gamma^2} \tag{5}$$

which has been derived in [8].

3. Comparison with experiments

The device tested is an index-guided buried heterostructure laser grown on an InP substrate with a width about 1 μm. The active region consists of five 105 Å $In_{0.55}Ga_{0.45}As_{0.88}P_{0.12}$ wells with 78 Å lattice matched InGaAsP barriers with a bandgap wavelength $\lambda_g = 1.28$ μm. The wells have 0.26% tensile strain. The multiple quantum wells are surrounded by InGaAsP spacer layers with the same composition as the barrier material. The total thickness of the InGaAsP region is about 2200 Å.

Amplified spontaneous emission from one facet of the laser was directed into a 1.25 m spectrometer and detected by a cooled germanium detector. Our measurements cover the the whole range of the spectrum including the transparency (zero modal gain) energy and a flat portion of the modal gain spectrum below the bandgap energy of the well region. The gain spectrum of the laser was measured based on the Hakki-Paoli method [9] for current biases below threshold. The intrinsic loss is determined by using the fact that the modal gain g_M approaches zero in the long wavelength limit.

The peak wavelength of each mode in the amplified spontaneous emission spectrum is a function of the refractive index. By comparing the peaks of two spectra of two different injection currents, the refractive index change due to the injection current difference is derived. The resonance conditions of two longitudinal modes are used to estimate the cavity length L. By using the formula from Adachi [10] at two wavelengths λ_1 and λ_2 for the refractive index of the waveguide core and InP cladding, the effective indices $n_e(\lambda_1)$ and $n_e(\lambda_2)$ can be determined by finding the propagation constant of the lowest waveguide mode. Choosing wavelengths from each end of our measurement range, $\lambda_1 \approx 1460$ nm and $\lambda_2 \approx 1590$ nm, we find the cavity length L to be 398 μm. The extracted effective

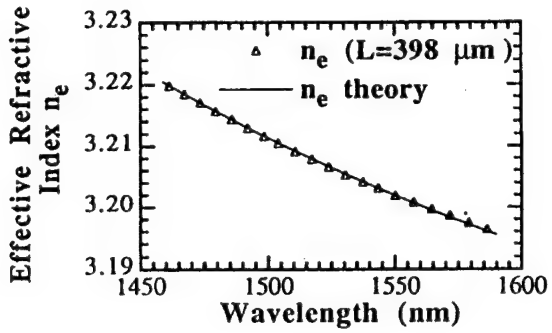

Figure 1. A plot of the measured dispersion of the effective index (triangles) and comparison with the theoretical effective index profile. From the experimental data and the theoretical fit, we obtain a cavity length of 398 μm.

index spectrum is shown in Fig. 1 as triangles. The solid line is the calculated effective index of the lowest (TE_0) mode of a slab waveguide, using Adachi's formula [10] for the refractive indices of the waveguide core and InP cladding. We can see from Fig. 1, that the solid line and the triangles match very well.

In Fig. 2, we show the measured and calculated TE polarized modal gain spectra at three different injection currents, 6, 8, and 10 mA. The bulk bandgap E_g and electron effective mass m_n used in our calculation for the $In_{1-x}Ga_xAs_yP_{1-y}$ are taken from [11]. The material parameters for GaAs, GaP, InAs, and InP are taken from [8, 11, 12]. The model-solid theory [12] is used for the bandgap offsets. The bandgap renormalization is taken into account by adding ΔE_g^{BGR} to the bulk bandgap E_g. We use [13] $\Delta E_g^{BGR} = -CN^{1/3}$, where C is a fitting parameter, to obtain the transparency energy position. The carrier densities are determined from the transparency energy corresponding to the quasi-Fermi level separation. The carrier densities are $N = 2.41$, 2.66, and 2.82×10^{18} cm^{-3}, for the three injection currents, 6, 8, and 10 mA, respectively. The bandgap renormalization coefficient is found to give a bandgap shift of -30 meV for a 2D carrier density 1×10^{12} cm^{-2}. The Γ for the tested laser is about 0.1, calculated directly from the waveguide theory. The experimental and theoretical results agree very well with each other. Note that only two fitting parameters, C and γ, are used, and the experimental spectra are explained very well with the full valence band-mixing model. The spectra show a clear blue-shift of the peak modal gain wavelength and a reduction of the differential modal gain ($\partial g_M / \partial I$) as the injection current is increasing. The blue-shift shows that the band-filling effect is larger than the bandgap renormalization.

In Fig. 3 we show the dispersions of both measured and calculated data for the induced refractive index change (Fig. 3(a)) and linewidth enhancement factor (Fig. 3(b)). Our model agrees well with the experimental refractive index change and linewidth enhancement spectra. Note that our formula (5) is a direct numerical evaluation of the refractive index profile and it automatically takes into account the Kramers-Kronig re-

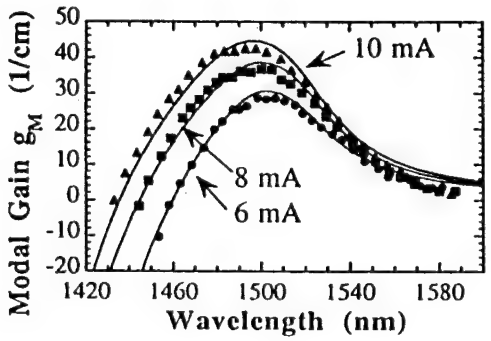

Figure 2. Our calculated (solid curves) and measured (symbols) modal gain spectra below threshold at I= 6, 8 and 10 mA using the Hakki-Paoli method.

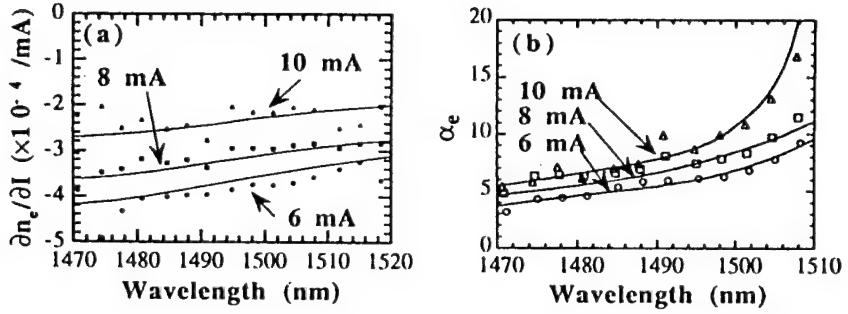

Figure 3. Comparison of our experimental data (symbols) and theoretical calculations (solid curves) for the (a) refractive index change per injection current change and (b) linewidth enhancement factor spectra.

lation and the scattering broadening mechanism. The refractive index decreases as the injection current increases. The magnitude of the refractive index change per unit injection current change is a decreasing function of the injection current.

The linewidth enhancement factor is proportional to the ratio of the refractive index change per injection current change and the differential modal gain profile. Since the refractive index change is roughly constant over the wavelength range of interest, the α_e spectrum is determined mainly by the differential gain profile. α_e tends to decrease at shorter wavelengths because of the increased differential gain caused by the band filling effects.

4. Conclusion

Theoretical models and experimental procedures for determining the gain, refractive i dex and linewidth enhancement factor from the Fabry-Perot peaks and peak shifts in th amplified spontaneous emission spectra of a strained InGaAsP quantum-well laser ha been presented. The gain and the refractive index profiles of a strained quantum-we laser structure can be extracted accurately by taking into account the optical confinemer factor. Furthermore, accurate monitoring of the differential gain and the Fabry-Per peak shift with injection current allows measurement of the linewidth enhancement fa tor, which has a direct impact on the high-speed modulation of semiconductor laser The excellent agreement between our theoretical results and experimental data verifi the material parameters and the quantum-well band structures used in our model.

Acknowledgements

The authors thank Drs. Y. K. Chen and T. Tanbun-Ek at AT&T Bell Laboratori for providing the laser. This work was supported by the U.S. Office of Naval Resear under Grant N00014-90-J1821. J. Minch was also supported by ONR AASERT Gra N00014-93-1-0844. W. Fang was supported by the AT&T Foundation Fellowship.

References

[1] Ahn D and Chuang S L 1988 *IEEE J. Quantum Electron.* **24** 2400

[2] O'Reilly E P and Adams A R 1994 *IEEE J. Quantum Electron.* **30** 366

[3] Chang C S and Chuang S L 1995 to appear on *IEEE J. Selected Topics in Quantu Electronic.*

[4] Henry C H 1982 *IEEE J. Quantum Electron.* **QE-18** 259

[5] Luttinger J M and Kohn W 1955 *Phys. Rev.* **97** 869

[6] Bir G L and Pikus G E 1974 *Symmetry and Strain-Induced Effects in Semiconduct* (New York: John Wiley)

[7] Chuang S L 1991 *Phys. Rev. B* **43** 9649

[8] Chuang S L 1995 *Physics of Optoelectronic Devices* (New York: Wiley)

[9] Hakki B M and Paoli T L 1973 *J. Appl. Phys.* **44** 4113

[10] Adachi S 1982 *J. Appl. Phys.* **53** 5863

[11] Hellwege K H 1982 *Landolt-Börnstein Numerical Data and Functional Relationships Science and Technology* **17a** (Berlin: Springer); 1986 **22a**

[12] Van de Walle C G 1989 *Phys. Rev. B* **39** 1871

[13] Tränkle G, Lach E, Forchel A, Scholz F, Ell C, Haug H and Weimann G 1987 *Phys. Re B* **36** 6712

CLEO® '96

Summaries of papers presented at the
Conference on Lasers and Electro-Optics

June 2–7, 1996
Anaheim Convention Center
Anaheim, California

Volume 9
1996 Technical Digest Series
Conference Edition

Sponsored by
Optical Society of America
IEEE/Lasers and Electro-Optics Society

In cooperation with
Quantum Electronics Division
of the European Physical Society
Japanese Quantum Electronics Joint Group

Optical Society of America
2010 Massachusetts Avenue NW
Washington DC 20036-1023

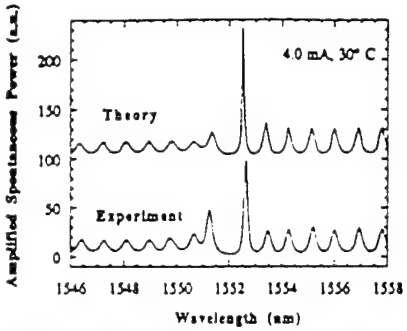

CMF6 Fig. 1 A plot of the amplified spontaneous emission spectrum taken at 30°C with an injection current of 4 mA (I_{th} = 4.7 mA). Theory is shown offset from the experimental data.

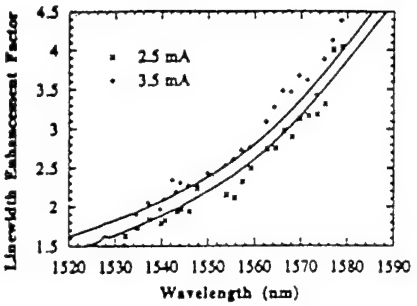

CMF6 Fig. 3 A plot of the linewidth enhancement factor at 30°C for various injection currents below threshold. Theoretical curves are given by the solid lines.

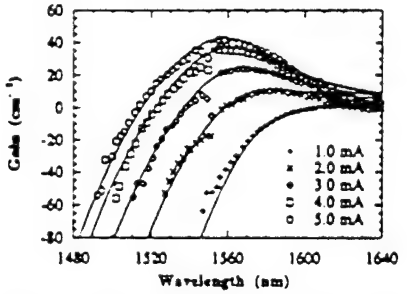

CMF6 Fig. 2 A plot of the modal gain measured at 30°C at various injection currents. The solid lines represent the theoretical fit.

CMF6 9:15 am

Theory and experiment on the amplified spontaneous emission from DFB lasers

J. Minch, C. S. Chang, W. Fang, S. L. Chuang, Y. K. Chen,* T. Tanbun-Ek,*
University of Illinois at Urbana/Champaign, Department of Electrical and Computer Engineering, 1406 W. Green St., Urbana, Illinois 61801

In the quest to improve distributed feedback lasers for telecommunication systems, it is critical to be able to characterize these lasers effectively. The amplified spontaneous emission of a laser biased below threshold provides a wealth of information and has been used in the past to characterize Fabry-Perot lasers.[1,2] In this paper, we use our model for the amplified spontaneous emission from DFB lasers coupled with our model for the material gain of strained quantum well lasers[3] to analyze data measured on a 1.55-μm InGaAsP/InGaAsP strained quantum well DFB laser in an effort to systematically extract important laser parameters.

The amplified spontaneous emission is modeled by treating the spontaneous emission as a current sheet, radiating in a DFB cavity with gain and arbitrary reflectors. The power emitted from each facet is found by solving the coupled-mode equations for the electric fields due to a delta-function source placed at an arbitrary position in the cavity. To obtain the full amplified spontaneous emission spectrum, this result is integrated over the length of the cavity to account for spontaneous emission throughout the device.

The device under study is a 1.55-μm buried heterostructure laser grown on an InP substrate. The active region is made of 1.6% compressively strained InGaAsP and the spectrum of this DFB laser, biased below threshold, was measured using a high-resolution 1.25-m spectrometer and a cooled germanium detector. Figure 1 shows the spectrum at 4.0 mA and 30°C near the stopband region. The theoretical fit with our model is shown offset from the experimental data.

The material gain of the laser is obtained from the amplified spontaneous emission spectrum in the spirit of the Hakki-Paoli method.[2] This method, however, is complicated by the fact that the periodic grating adds an effective mirror loss term, which depends quite strongly on wavelength, particularly near the stop band (lasing) region. This effective mirror loss term can have the effect of enhancing the gain on one side of the stop band and degrading the gain on the other side. Figure 2 shows the modal gain coefficient as a function of photon energy at several current levels up to threshold (I_{th} = 4.7 mA) at a temperature of 30°C. The solid lines give a theoretical fit. Noting that the DFB mirror loss term is a very weak function of current injection, the differential gain is easily obtained by taking the difference between gain curves measured a small current level apart.

The peak positions of the spectrum are subsequently measured over the current range up to threshold and used to obtain a spectrum for the current induced effective index shift. By taking the ratio of index shift to differential gain, we obtain the linewidth enhancement factor.[4] Figure 3 shows the linewidth enhancement factor for this laser at different injection currents below threshold. Solid lines show the theoretical fit of the data.

In summary, use of the amplified spontaneous emission spectrum to extract key material parameters from a distributed feedback laser biased below threshold is demonstrated both theoretically and experimentally.

*AT&T Bell Laboratories, 600 Mountain Ave., Murray Hill, New Jersey 07974

1. C. S. Chang, S. L. Chuang, J. Minch, W. Fang, Y. K. Chen, T. Tanbun-Ek, IEEE J. Quantum Electron., in press.
2. B. W. Hakki, T. L. Paoli, J. Appl. Phys. 44, 4113 (1973).
3. C. S. Chang, S. L. Chaung, IEEE J. Selected Topics in Quantum Electron. 1, 218 (1995).
4. C. H. Henry, IEEE J. Quantum Electron. 18, 259 (1982).

CLEO® '96

Summaries of papers presented at the
Conference on Lasers and Electro-Optics

June 2–7, 1996
Anaheim Convention Center
Anaheim, California

Volume 9
1996 Technical Digest Series
Conference Edition

Sponsored by
Optical Society of America
IEEE/Lasers and Electro-Optics Society

In cooperation with
Quantum Electronics Division
of the European Physical Society
Japanese Quantum Electronics Joint Group

Optical Society of America
2010 Massachusetts Avenue NW
Washington DC 20036-1023

CWR6 5:45 pm

Measurement of spatially dependent carrier lifetimes in 1.55-μm DFB quantum well lasers using microwave modulation

W. Fang, C. G. Bethea,* Y. K. Chen,* T. Tanbun-Ek,* S. L. Chuang,** *Department of Electrical and Computer Engineering, University of Illinois at Urbana-Champaign, 1406 West Green Street, Urbana, Illinois 61801*

We study the effect of a distributed feedback (DFB) structure on the carrier lifetime in a semiconductor laser. In DFB lasers, the spatially inhomogeneous optical intensity along the longitudinal direction of the active region gives rise to spatial hole burning. We show that this inhomogeneous intensity also creates a spatially dependent differential carrier lifetime, and that this spatial dependence exists even when the laser is biased below threshold. The differential carrier lifetimes are measured from the intrinsic microwave modulation responses for a laser biased below threshold.

The laser diodes tested are 1.55 μm DFB lasers with an InGaAsP/InGaAsP multiple quantum well active region on an InP substrate. The dimensions of the active stripe are approximately 300 μm in length and 1-μm wide. The typical threshold of these lasers is 9 mA at room temperature. The front facet is antireflection (AR) coated and the rear facet is high-reflection (HR) coated to maximize the power output from the front facet.

The optical intensity profile of a DFB laser is obtained by measuring the spatial dependence of the spontaneous emission (SE) spectrum above threshold.[1] Spatial hole burning in the 1.55-μm DFB laser is demonstrated in Fig. 1. The growth of the SE at the front (AR facet) and the saturation of the SE at the rear (HR facet) of the laser cavity indiates that the optical intensity is higher at the rear than the front.

The intrinsic modulation response is measured using optical injection of microwave-modulated carriers directly into the quantum-well region of the laser.[2,3] Optical pumping of the 1.55-μm DFB laser is achieved using an externally modulated 1.3-μm Fabry-Perot laser. The wavelength of the pump laser corresponds to an energy near the top of the quantum wells. The pump light is injected into the laser through one of the facets where it is strongly absorbed within a short distance, even when the laser is under current injection. Thus, spatially selective pumping of the active region is obtained depending on which facet (either HR or AR) is pumped. The modulated output of the 1.55-μm laser is collected from the opposite facet and detected using a high-speed photodetector. The intrinsic modulation responses are measured as a function of applied currents to the laser using a microwave spectrum analyzer.

The microwave modulation response of the amplified spontaneous emission (ASE) for a 1.55-μm DFB laser biased below threshold is shown in Fig. 2 for both front and rear pumping. A theoretical fit (solid lines) accompanies the measured data (symbols). The theoretical fit is obtained by solving the small-signal rate equations of a laser biased below threshold. There are no observed resonances in the ASE modulation response, and only an RC-type rollover is exhibited. In addition, the modulation responses are not similar at currents near threshold. This is because the rate of stimulated emission is not the same throughout the cavity due to the inhomogeneous intensity profile inside an HR/AR coated DFB laser. We add, however, that when the laser is biased above threshold the modulation response is dominated by the cavity resonance, and then the resonance frequencies are observed and are independent of the pumping position.

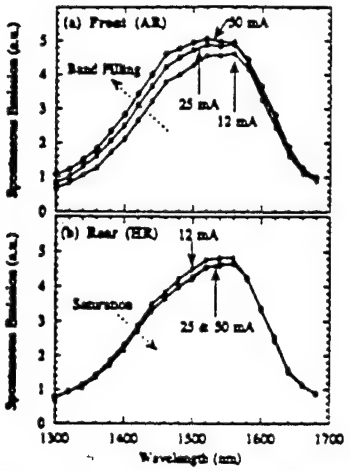

CWR6 Fig. 1 Measurement of spatial hole burning in DFB lasers. The spontaneous emission at (a) the front of the laser continues to grow while that at (b) the rear of the laser is saturated due to a high optical intensity.

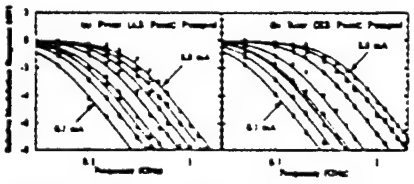

CWR6 Fig. 2 Intrinsic microwave modulation responses for injected currents of 0.1, 0.4, 0.7, 1.0, 2.0, 4.0, 6.0, and 8.0 mA for (a) front (AR facet) pumped and (b) rear (HR facet) pumped cases. The threshold current is 9 mA.

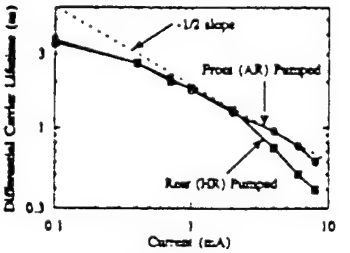

CWR6 Fig. 3 The differential carrier lifetime versus injected current for front (AR facet) and rear (HR facet) pumping. The threshold current is 9 mA.

The differential carrier lifetime is extracted from the theoretical fit of the intrinsic modulation response. The differential carrier lifetime is plotted versus the applied current in Fig. 3. As shown, the differential carrier lifetime, and hence the carrier lifetime, at the front (AR-coated side) of the laser is longer than that at the rear (HR-coated side) when the laser is biased near threshold. This is consistent with Fig. 1 where the stimulated emission is stronger at the rear than the front. For intermediate values of current, the slope of the differential lifetime versus current is approximately −1/2 on a log-log plot, which agrees with the $J/ed = Bn^2$ law for radiative recombination.[4] For very small currents, the slope flattens due to defect and single-carrier recombination. At currents very close to threshold, the slope approaches −1, especially at the rear, and shows that stimulated emission is beginning to dominate the carrier recombination process.

The measured modulation responses of the ASE, which vary with pumping position, indicate a spatially dependent carrier lifetime below threshold. The carrier lifetime measurements are in agreement with the measurements of the spatial hole burning and the optical intensity profile. The carrier lifetime is a function of current injection, and we show that it is dominated by radiative recombination (both spontaneous and stimulated). With increasing carrier density, the spontaneous emission rate increases, thereby reducing the carrier lifetime. Near threshold, the carrier lifetime is reduced further in regions where the optical intensity is stronger due to a faster stimulated emission rate.

*AT&T Bell Laboratories, 600 Mountain Avenue, Murray Hill, New Jersey 07974
**Department of Electrical and Computer Engineering, University of Illinois at Urbana-Champaign, 1406 West Green Street, Urbana, Illinois 61801

1. W. Fang, C. G. Bethea, Y. K. Chen, S. L. Chuang, IEEE J. Sel. Top. Quantum Electron. 1, 117 (1995).
2. C. E. Zah, M. C. Wang, R. Bhat, T. P. Lee, S. L. Chuang, Z. Wang, D. Darby, D. Flanders, J. J. Hsieh, International Conference on Semiconductor Lasers, 1993, Hawaii.
3. D. Vassilovski, T. C. Wu, S. Kan, K. Y. Lau, C. E. Zah, IEEE Photon. Technol. Lett. 7, 706 (1995).
4. S. L. Chuang, *Optoelectronics and Integrated Optics* (Wiley, New York, 1995).

Amplified Spontaneous Emission Spectroscopy in Strained Quantum-Well Lasers

Chih-Sheng Chang, *Student Member, IEEE*, Shun Lien Chuang, *Senior Member, IEEE*, Jeffrey R. Minch, Wei-chiao W. Fang, *Student Member, IEEE*, Y. K. Chen, *Senior Member, IEEE*, and T. Tanbun-Ek

***Abstract*—Amplified spontaneous emission spectroscopy is used to extract the gain and refractive index spectra systematically. We obtain the gain and differential gain spectra using the Hakki–Paoli method. The refractive index profile, the induced change in refractive index by an incremental current, and the linewidth enhancement factor are measured from the Fabry–Perot peaks and the current-induced peak shifts in the amplified spontaneous emission spectra. The measured optical gain and refractive index are then compared with our theoretical model for strained quantum-well lasers. We show that a complete theoretical model for calculating the electronic band structure, the optical constant, and the linewidth enhancement factor agrees very well with the experiment. Our approach demonstrates that amplified spontaneous emission spectroscopy can be a good diagnostic tool to characterize laser diodes, extract the optical gain and index profiles, and confirm material parameters such as the strained quantum-well band structure parameters for a semiconductor structure under carrier injection.**

I. Introduction

In recent years, strained quantum-well lasers have been shown to demonstrate higher performance over their lattice-matched counterparts in terms of reduced threshold current density, high temperature operation, and high-speed modulation [1], [2]. Some of the most important parameters affecting the performance of high-speed semiconductor lasers include the optical gain spectrum, the refractive index change with injected current, and the linewidth enhancement factor [3]. Although semiconductor lasers have been developed with record breaking direct modulation speeds, communication systems cannot utilize the full bandwidth of the laser due to its large linewidth enhancement factor or chirp. The linewidth enhancement factor increases the dispersion and limits the maximum bit rate of long-distance fiber optic communication networks. It depends crucially upon the differential gain and current induced change in the refractive index. Intensive research has been devoted to both maximizing the differential gain and minimizing the change of refractive index in semiconductor lasers in order to reduce the linewidth enhancement factor [4]–[7].

Theoretical models for the gain and refractive index change for strained quantum-well lasers have been developed [8]–[11] recently. However, not much experimental work has been compared with theoretical models which take into account valence band-mixing effects in a strained quantum-well structure. The reasons are probably due to the fact that many material parameters in strained InGaAsP quaternary compounds such as the effective mass parameters, the deformation potentials, and the optical refractive indices have not all been determined experimentally. Most of these parameters are interpolated from the parameters of the bulk binary or ternary compounds. If the linear interpolation formulas can give reasonable agreement with experimental data, then theoretical models using these material parameters can certainly provide useful information on optimizing the design of various optoelectronic devices.

We present a comprehensive theoretical model for the amplified spontaneous emission, gain, and refractive index spectra of a strained InGaAsP quantum-well laser, designed for applications in long-wavelength 1.55 μm communication systems, in Section II. The spontaneous emission intensity is modeled using an equivalent electric current source of radiation and is calculated directly from Maxwell's equations in the presence of gain. We then discuss our experimental procedures in Section III for the gain measurements, based on the Hakki–Paoli method [12], and the extraction of the refractive index profile and the linewidth enhancement factor [13]. We compare our theoretical calculations with the measured gain, refractive index change, and the linewidth enhancement factor profiles in Section IV and present our conclusions in Section V. We demonstrate that our theoretical model and experimental procedures for the amplified spontaneous emission spectroscopy provide a very sensitive diagnostic tool to investigate a strained semiconductor quantum well in the presence of carrier injection by a forward voltage bias.

II. Theory

A. Amplified Spontaneous Emission Spectroscopy

The spontaneous emission is modeled as a distribution of uniform current sheets along the longitudinal direction inside the laser diode. We consider a current sheet $-\hat{x}J_s\delta(z - z_s)$

Manuscript received March 6, 1995; revised August 3, 1995. The work done at the University of Illinois was supported by the U.S. Office of Naval Research under Grant N00014-90-J1821. J. R. Minch was supported by ONR AASERT Grant N00014-93-1-0844. W. Fang was supported by the AT&T Foundation Fellowship.

C.-S. Chang, S. L. Chuang, J. Minch, and W.-c. Fang are with the Department of Electrical and Computer Engineering, University of Illinois at Urbana-Champaign, 1406 W. Green Street, Urbana, IL 61801 USA.

Y. K. Chen and T. Tanbun-Ek are with AT&T Bell Laboratories, Murray Hill, NJ 07974 USA.

IEEE Log Number 9415321.

radiating in a bulk semiconductor with refractive index n. The power radiated to the right due to the current sheet is

$$P_t = A\frac{\eta}{8}|J_s|^2, \tag{1}$$

where A is the area of the current sheet and η is the characteristic impedance of the semiconductor, i.e., $\eta = (\mu_o/\epsilon)^{1/2} = \eta_o/n$ where $\eta_o = (\mu_o/\epsilon_o)^{1/2} = 377\ \Omega$ is the characteristic impedance of free space. We compare this to the radiated power due to the spontaneous emission of photons with energy between $\hbar\omega$ and $\hbar\omega + \Delta E$ within a thin layer between z_s and $z_s + dz_s$, given by

$$\begin{aligned} P_t &= W(\hbar\omega)A\,dz_s \\ &= \frac{\beta}{2}r_{sp}(\hbar\omega)\,\Delta E\hbar\omega A\,dz_s, \end{aligned} \tag{2}$$

where β is the fraction of the spontaneous events that are coupled into the waveguide mode, $r_{sp}(\hbar\omega)\,\Delta E$ is the spontaneous emission rate per unit volume of photons with energy between $\hbar\omega$ and $\hbar\omega + \Delta E$, and A is the cross-sectional area. The factor of 1/2 accounts for the emission in the $+z$ direction. From (1) and (2), we can model the spontaneous events within the thin layer as a current sheet with

$$|J_s|^2 = \frac{8}{\eta}W(\hbar\omega)\,dz_s. \tag{3}$$

Equation (3) gives a direct relation between the spontaneous emission and an equivalent current sheet as the optical radiation source at position z_s.

To model the spontaneous emission of a laser, the equivalent current sheet is placed in a cavity, which provides feedback and mode selection. In a Fabry–Perot cavity as shown in Fig. 1, the fields due to the equivalent current sheet can be described as

$$\begin{aligned} \boldsymbol{E}_I &= \hat{x}E_1(r_1e^{ik_onz} + e^{-ik_onz}) \\ &\qquad \text{for} \quad 0 < z < z_s \end{aligned} \tag{4}$$

$$\begin{aligned} \boldsymbol{E}_{II} &= \hat{x}E_2[e^{ik_on(z-L)} + r_2e^{-ik_on(z-L)}] \\ &\qquad \text{for} \quad z_s < z < L, \end{aligned} \tag{5}$$

where $k_o = 2\pi/\lambda$, λ is the wavelength in free space, r_1 (r_2) is the field reflection coefficient for the left (right) mirror, and L is the cavity length. Note that $r_1 = r_2 = (n-n_o)/(n+n_o)$ for a symmetric cavity and power conservation requires that $|r_2|^2+(n_o/n)|t_2|^2 = 1$, where $n_o = 1$ is the refractive index of free space and $t_2 = 1 + r_2$ is the field transmission coefficient. Also, the power reflectivity is $R = |r_2|^2$. By matching the boundary conditions for the tangential electric and magnetic fields at $z = z_s$, E_2 is found to be

$$E_2 = \frac{\eta J_s}{2}e^{-ik_on(z_s-L)}\left(\frac{1+r_1e^{i2k_onz_s}}{1-r_1r_2e^{i2k_onL}}\right). \tag{6}$$

The output intensity of photons with energy between $\hbar\omega$ and $\hbar\omega + \Delta E$ due to the layer dz_s emitted from the right facet can

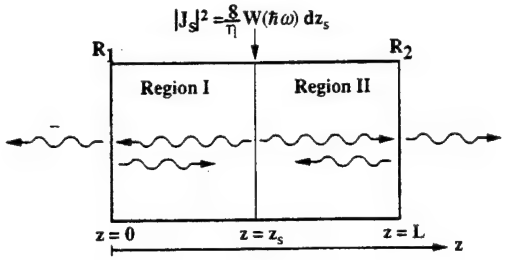

Fig. 1. A schematic configuration showing the amplified spontaneous emission from an equivalent current sheet as the source of spontaneous emission at position $z = z_s$. The total emission intensity is the integrated amplified intensity over the source distribution z_s along the longitudinal direction of the laser cavity.

be obtained from $E_t = (1 + r_2)E_2$ at $z = L$ and

$$\begin{aligned} I(z_s, \hbar\omega) &= \frac{1}{2\eta_o}|(1+r_2)E_2|^2 \\ &= \frac{\eta^2}{8\eta_o}|1+r_2|^2|J_s|^2 \\ &\quad \times\left[\frac{1+r_1e^{Gz_s}\cos(2k_on_ez_z)+e^{2Gz_s}|r_1|^2}{|1-r_1r_2e^{GL}e^{i2k_on_eL}|^2}\right]e^{G(L-z_s)}, \end{aligned} \tag{7, 8}$$

where the waveguide modal field and the presence of gain are taken into account by replacing the propagation constant k_on with $k_on_e - iG/2$. n_e is the effective index of the waveguide mode, and G is the net gain of the active medium. In a laser diode, $G = g_M - \alpha_i$, where g_M is the modal gain and α_i is the intrinsic loss. Since $I(z_s, \hbar\omega)$ is the intensity generated by $|J_s|^2$ due to a finite sheet width dz_s as given in (3), the total amplified spontaneous intensity emitted from the right facet is found by integrating the intensity $I(z_s, \hbar\omega)$ over the entire cavity,

$$\begin{aligned} I_{\text{ASE}}(\hbar\omega) &= \int_0^L I(z_s, \hbar\omega)\,dz_s \qquad (9) \\ &= (1-R)\left[\frac{W(\hbar\omega)L}{GL}\right]\frac{(e^{GL}-1)(1+Re^{GL})}{|1-Re^{GL}e^{i2k_on_eL}|^2}. \qquad (10) \end{aligned}$$

where we have used $r_1 = r_2 = \sqrt{R}$ and neglected the terms with a $1/(k_on_e)$ prefactor since $k_on_e \gg G$. By using the fact that G is a slowly varying function of wavelength as compared to the fast varying function $e^{i2k_on_eL}$, we obtain the ratio between adjacent maxima and minima of I_{ASE}

$$\frac{I_{ASE,\,\max}}{I_{ASE,\,\min}} = \left|\frac{1+Re^{GL}}{1-Re^{GL}}\right|^2. \tag{11}$$

This result is used in Section III to extract the gain spectrum G from the amplified spontaneous emission spectrum using the Hakki–Paoli method. Note that a peak wavelength of a Fabry–Perot mode in the amplified spontaneous emission spectrum occurs when

$$2\pi\frac{n_e}{\lambda}L = m\pi, \tag{12}$$

where m is the mode number. The procedure to extract the effective index $n_e(\lambda)$ and the induced change in the effective index due to current injection will be discussed in Section III.

B. Gain and Refractive Index Model

The subband structure and the corresponding wave functions of the active region are solved by the effective mass theory [14]. The theory of Bir–Pikus [15] is used to take into account the effects of strain, and the effective mass equation is solved by a finite difference method [11]. The spontaneous emission rate $r_{sp}(\hbar\omega)$ for a single quantum-well can be calculated as

$$r_{sp}(\hbar\omega) = \frac{n_e^2\omega^2}{\pi^2\hbar c^2}\frac{(2g_{sp}^{\mathrm{TE}} + g_{sp}^{\mathrm{TM}})}{3} \tag{13}$$

$$g_{sp}^{p}(\hbar\omega) = \frac{q^2\pi}{n_e c\epsilon_o m_o^2\omega L_z}\sum_{n,m}\int |\mathrm{M}_{nm}^{p}(k_t)|^2 \cdot \frac{f_n^c(k_t)[1 - f_m^v(k_t)]\left(\frac{\gamma}{\pi}\right)}{[E_{nm}^{cv}(k_t) - \hbar\omega]^2 + \gamma^2}\frac{k_t\,dk_t}{2\pi}. \tag{14}$$

where q is the magnitude of the electron charge, $\hbar$ is Planck's constant divided by 2π, c is the speed of light in free space, m_o is the electron rest mass, L_z is the well width, γ is the Lorentzian half-linewidth, f_n^c (f_m^v) is the Fermi occupation probability for electrons in the n_{th} (m_{th}) conduction (valence) subband, and E_{nm}^{cv} is the transition energy between the n_{th} conduction and m_{th} valence subbands. The superscript p in (14) stands for polarization, $p = \mathrm{TE} = x$ or y and $p = \mathrm{TM} = z$. The momentum matrix elements M^p for the TE and TM polarizations are

$$|\mathrm{M}_{nm}^{\mathrm{TE}}|^2 = \frac{\mathrm{M}_b^2}{4}\{|\langle g_{m,lh} + \sqrt{2}g_{m,so}|\phi_n\rangle|^2 + 3|\langle g_{m,hh}|\phi_n\rangle|^2\}. \tag{15}$$

$$|\mathrm{M}_{nm}^{\mathrm{TM}}|^2 = \mathrm{M}_b^2\left|\left\langle g_{m,lh} - \frac{1}{\sqrt{2}}g_{m,so}|\phi_n\right\rangle\right|^2. \tag{16}$$

where ϕ_n is the conduction band envelope function, $g_{m,hh}$, $g_{m,lh}$, and $g_{m,so}$ are the heavy-hole, light-hole, and spin-orbit split-off band components of the m_{th} valence envelope function, and

$$\mathrm{M}_b^2 = \frac{m_o E_p}{6} = \frac{|\langle S|p_x|X\rangle|^2}{3} \tag{17}$$

is the bulk value of the momentum matrix element. E_p is an energy parameter which can be found in [16]. Universal curves for momentum-matrix elements of the TE and TM polarizations of strained quantum-well lasers as a function of strain have been presented recently [17] using an infinite barrier model.

The material gain can be determined from the spontaneous emission rate [18] using

$$g = g_{sp}^{p}\left[1 - \exp\left(\frac{\hbar\omega - \Delta F}{k_B T}\right)\right] \tag{18}$$

for $p = \mathrm{TE}$ or TM, and the modal gain $g_M = \Gamma g$ is obtained by multiplying the material gain by the optical confinement factor Γ. The optical confinement factor Γ is the optical confinement of the waveguide mode weighted by $n_w L_z/W_{mode}$, where n_w is the number of wells and W_{mode} is effective width of the waveguide mode. The confinement factor of the waveguide mode is calculated using the core dimension d, which is the total thickness of the well, barrier, and spacer layers, and the refractive indices $n(\lambda)$ of the bulk InGaAsP spacer layer and the InP cladding layer.

The induced change in the effective refractive index due to interband transitions is

$$\delta n_e(\hbar\omega) = \Gamma\frac{q^2\hbar^2}{n_e m_o^2 L_z\epsilon_0}\sum_{n,m}\int \frac{k_t\,dk_t}{2\pi}|\mathrm{M}_{nm}^{p}(k_t)|^2 \cdot \frac{[E_{nm}^{cv}(k_t) - \hbar\omega]}{E_{nm}^{cv}(k_t)[E_{nm}^{cv}(k_t) + \hbar\omega]} \cdot \frac{[f_n^c(k_t) - f_m^v(k_t)]}{[E_{nm}^{cv}(k_t) - \hbar\omega]^2 + \gamma^2}. \tag{19}$$

which has been derived in [19], [20]. It should be pointed out that the optical confinement factor Γ for the quantum-well active layer appears in both the modal gain g_M and the induced effective index change δn_e. Note that the effective index n_e as a function of the carrier density N can be written as $n_e(N) = n_e(N = 0) + \delta n_e$ and usually δn_e is much smaller than $n_e(N = 0)$.

The linewidth enhancement factor, which determines the semiconductor laser linewidth and plays an important role in the high-speed direct modulation of lasers, can then be obtained by [3]

$$\alpha_e = -\frac{4\pi}{\lambda}\frac{\frac{\partial\delta n_e}{\partial N}}{\frac{\partial g_M}{\partial N}}, \tag{20}$$

where $\partial g_M/\partial N$ is the differential gain and $\partial\delta n_e/\partial N$ is incremental change in the effective index due to carrier injection. Both quantities can be approximated by first calculating (18) or (19) at two nearby carrier densities, and then finding the ratio of the differences. Note that the effect of the optical confinement factor Γ is cancelled in (20). Both a large differential gain and a small $\partial\delta n_e/\partial N$ can reduce the linewidth enhancement factor α_e.

III. Experiments

The device tested is a buried heterostructure laser grown on an InP substrate, designed for applications in long-wavelength 1.55 μm communication systems. The active region consists of five strained InGaAsP quantum wells with InGaAsP barriers. The well width and strain are 105 Å and 0.26% tensile, respectively, and the PL wavelength is near 1.485 μm. The lattice matched InGaAsP barriers are 78 Å thick with a bandgap wavelength $\lambda_g = 1.28$ μm. The multiple quantum wells are surrounded by InGaAsP spacer layers with the same composition as the barrier material. The entire InGaAsP region is sandwiched by n- and p-doped InP layers which provide the electrical injection. The bandedge profile of the laser structure is shown in Fig. 2. The total thickness of the InGaAsP region is about 2200 Å and its width is about 1 μm.

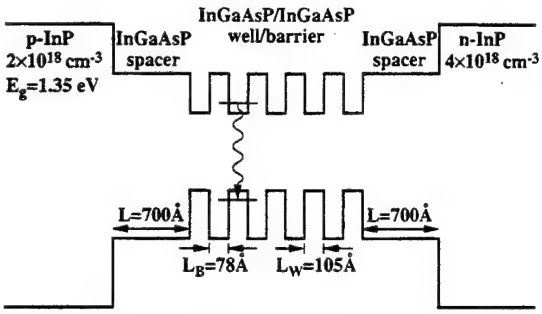

Fig. 2. The conduction and valence band edge profiles for the InGaAsP strained quantum-well laser structure under study. The InGaAsP well region is slightly tensile strained with a PL wavelength of 1.485 μm. The barrier InGaAsP regions are lattice-matched to InP and its bandgap wavelength is 1.28 μm.

Amplified spontaneous emission measurements are taken using a 1.25 m spectrometer and a cooled germanium detector. The laser is mounted on a thermoelectric cooler plate. The thermal effects which would have resulted in a red shift of the bandgap energy have been removed by using a thermoelectric temperature controller to keep the temperature of the thermoelectric cooler plate at a constant, 25°C. The data acquisition procedure to extract the peak wavelengths in the amplified spontaneous emission spectrum is tedious and a high-resolution spectrometer is required. In Fig. 3(a), we show a typical detected amplified spontaneous emission signal. A small portion of the spectrum is enlarged in Fig. 3(b) to compare the change in the amplified spontaneous emission spectrum with injection current. The peaks exhibit a blue shift in the presence of a larger injection current.

The gain spectrum of the laser is measured based on the Hakki–Paoli method [12] for current biases below threshold. The modal gain is obtained from the peaks $[I_{\max}(\lambda)]$ and valleys $[I_{\min}(\lambda)]$ of the longitudinal Fabry–Perot modes,

$$g_M(\lambda) = \alpha_i + \frac{1}{L} \ln \frac{Q(\lambda)}{R}, \tag{21}$$

where

$$Q(\lambda) = \frac{I_{\max}^{1/2}(\lambda) - I_{\min}^{1/2}(\lambda)}{I_{\max}^{1/2}(\lambda) + I_{\min}^{1/2}(\lambda)}. \tag{22}$$

Note that the detected signal I is proportional to the total amplified spontaneous emission intensity $I_{\mathrm{ASE}}(\hbar\omega)$ derived in (10). The above modal gain formula (21) is equivalent to (11).

Using the fact that g_M approaches zero in the long wavelength limit ($\lambda = \infty$, i.e., far below the bandgap) and R is a weak function of wavelength within the range of measurement, we obtain

$$g_M(\lambda) = \frac{1}{L} \ln \frac{Q(\lambda)}{Q(\infty)}. \tag{23}$$

The peak wavelengths of the Fabry–Perot modes are accurately determined by fitting each peak region, consisting of three sampled points, the local maximum and its two neighbors, to a parabola. The peak wavelength of each mode in the amplified spontaneous emission spectrum is a function of the refractive index. Using (12) and taking into account the

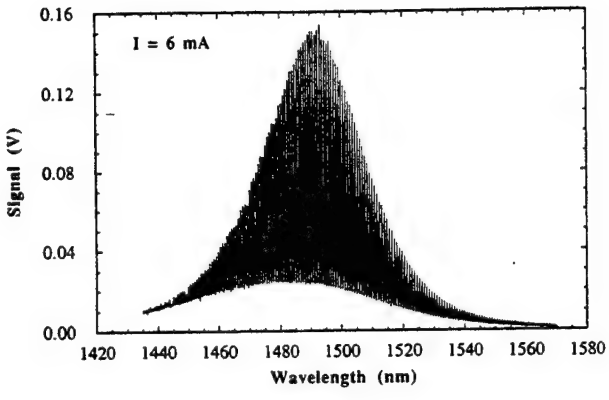

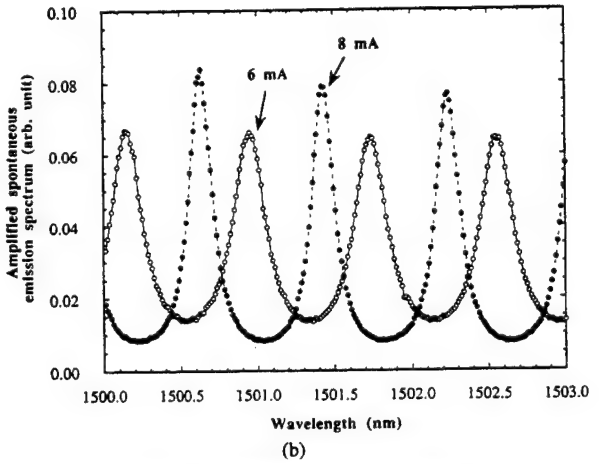

Fig. 3. (a) The amplified spontaneous emission spectrum below lasing threshold showing minima and maxima due to the Fabry–Perot modulation of the emission intensity. (b) An expanded region of (a) at two currents, $I = 6$ and 8 mA, showing the blue shifts of the peak wavelengths with increasing current.

dispersion of $n_e(\lambda)$, the change in the refractive index can be determined from

$$\Delta n_e = \frac{\lambda}{2L} \frac{\Delta\lambda_s}{\Delta\lambda_m}, \tag{24}$$

where $\Delta\lambda_s$ is the wavelength shift of a Fabry–Perot mode due to a change in injected carriers and $\Delta\lambda_m$ is the Fabry–Perot mode spacing.

The linewidth enhancement factor can then be extracted using

$$\alpha_e = 2\pi \frac{\Delta\lambda_s}{\Delta\lambda_m} \frac{1}{\Delta\left[\ln \dfrac{Q(\lambda)}{Q(\infty)}\right]}, \tag{25}$$

where $\Delta\{\ln[Q(\lambda)/Q(\infty)]\}$ is the change in $g_M(\lambda)L$ due to a change in injected carriers. Note that the above formula is independent of the cavity length L. In general, α_e varies with wavelength and the injection current density.

IV. Comparison Between Theory and Experiment

In order to obtain the cavity length, we present a systematic method to estimate the cavity length from the peak positions

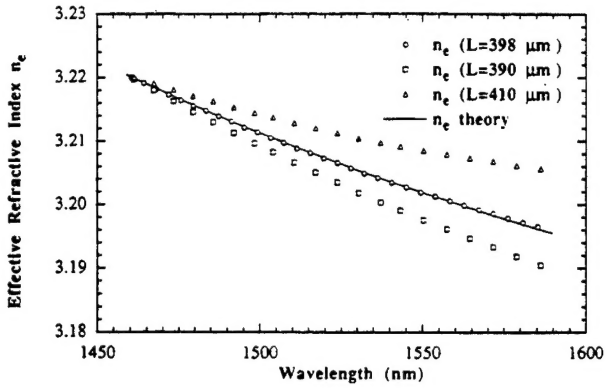

Fig. 4. A plot of the measured effective index (circles) from the mode spacings in Fig. 3 as a function of wavelength and comparison with the theoretical effective index profile using the refractive index profile from [21] for the InGaAsP core layer and the InP cladding. From the experimental data and the theoretical fit, we obtain a cavity length of 398 μm. The data given by the rectangles and triangles are for different cavity lengths $L = 410$ and 390 μm, respectively.

in the amplified spontaneous emission spectrum. Consider two peaks at λ_1 and λ_2 with effective indices $n_e(\lambda_1)$ and $n_e(\lambda_2)$, respectively. The cavity length L is given by

$$L = \frac{\Delta m}{2\left[\dfrac{n_e(\lambda_1)}{\lambda_1} - \dfrac{n_e(\lambda_2)}{\lambda_2}\right]}. \tag{26}$$

where $\Delta m = m_1 - m_2$ is the number of modes between λ_1 and λ_2 and $m_i = 2n_e(\lambda_i)L/\lambda_i$.

By using the formula from Adachi [21] for the refractive index of a quaternary InGaAsP semiconductor, we find the refractive indices for the waveguide layer and the InP substrate at both wavelengths λ_1 and λ_2. The effective indices $n_e(\lambda_1)$ and $n_e(\lambda_2)$ can then be determined by calculating the propagation constant of the lowest waveguide mode. Choosing wavelengths from each end of our measurement range, $\lambda_1 \approx 1460$ nm and $\lambda_2 \approx 1590$ nm, we find the cavity length L to be 398 μm using (26). The cavity length is also estimated to be about 380 ± 20 μm by direct measurement under a microscope. Our method of extracting the L from (26) agrees very well with the direct measurement. After determining the cavity length, the longitudinal mode number m_1, and hence every m, is known. Then, the effective index can be extracted for each mode m in the amplified spontaneous emission spectrum using (12). The extracted effective index spectrum is shown in Fig. 4 as circles. The solid line is the calculated dispersion of the effective index $n_e(\lambda)$ of the lowest (TE_0) mode of a waveguide that corresponds to the waveguide of the laser tested, using Adachi's formula [21] for the refractive indices of the waveguide core and InP cladding. We can see from Fig. 4, that the solid line and the circles match very well. Also shown are the extracted effective index profiles by assuming two arbitrary cavity lengths, 390 and 410 μ m. These two curves are plotted to demonstrate the sensitivity of our estimate of the cavity length. From these curves, this method is found to be able to give an estimation of L within 2 μ m. The overall fit of the effective index profile $n_e(\lambda)$ serves as a self-consistent check of the validity of our method.

TABLE I
THE MATERIAL PARAMETERS USED FOR THE CALCULATIONS [16]

$In_{1-x}Ga_xAs_yP_{1-y}$ well	x=0.45, y=0.88
Bandgap E_g (eV)	$1.35 + 0.642x - 1.101y + 0.758x^2$ $+0.101y^2 - 0.159xy - 0.28x^2y + 0.109xy^2$
Electron effective mass m_n/m_o	$0.08 - 0.116y + 0.026x + 0.06y^2$ $+0.064x^2 - 0.059xy + 0.032y^2x - 0.02yx^2$
$In_{1-x}Ga_xAs_yP_{1-y}$ lattice matched to InP	$x = \frac{0.1894y}{0.4184 - 0.013y}$
Bandgap E_g (eV)	$1.35 - 0.775y + 0.149y^2$
Electron effective mass m_n/m_o	$0.08 - 0.039y$

* The quaternary interpolation formula, $P(In_{1-x}Ga_xAs_yP_{1-y}) = xy\ P(GaAs) + x(1-y)\ P(GaP) + (1-x)y\ P(InAs) + (1-x)(1-y)\ P(InP)$ is used for the Luttinger parameters γ_1, γ_2, and γ_3, spin-orbit split-off energy Δ, and the energy parameter E_p (see Eq. (17)). The material parameters for GaAs, GaP, InAs, and InP are taken from [16], [19], [22], and listed in Table II.

TABLE II
MATERIAL PARAMETERS FOR BINARY COMPOUND SEMICONDUCTORS [16], [19], [22]

	GaAs	InAs	GaP	InP
γ_1	6.80	20.4	4.05	4.95
γ_2	1.90	8.30	0.49	1.65
γ_3	2.73	9.10	1.25	2.35
Spin-orbit energy Δ (eV)	0.34	0.38	0.08	0.11
Energy parameter E_p (eV)	25.7	22.2	22.2	20.4

We also compare our measurements of the gain spectrum with our theoretical model. The laser described in Section III is modeled using the band structure and laser gain theory presented in Section II. The bandgap offsets are determined from the model-solid theory [22]. When applying the theory, we assume that the quaternary $In_{1-x}Ga_xAs_yP_{1-y}$ can be treated as a compound consisting of a binary compound InP and a ternary compound. We use $In_{1-x}Ga_xAs_yP_{1-y} = (1-x)\ InP + x\ GaAs_{y/x}P_{1-y/x}$ for $x > y$ and $In_{1-x}Ga_xAs_yP_{1-y} = (1-y)\ InP + y\ In_{1-x/y}Ga_{x/y}As$ for $x < y$. The material parameters used in our calculations are summarized in Tables I and II. The bandgap offsets without the strain deformation potentials for the laser tested are found to be 44 meV for the conduction band and 100 meV for the valence band. The bandgap renormalization is taken into account by adding ΔE_g^{BGR} to the bulk bandgap E_g listed in Table I. We use [23] $\Delta E_g^{BGR} = -CN^{1/3}$, where C is a fitting parameter. The calculated valence subband structure is shown in Fig. 5(a). The TE and TM matrix elements for the C1-HH1 and C1-LH1 transitions are shown in Fig. 5(b). Because the quantum wells are only slightly tensile strained, the strain-induced upward shift of the light-hole bandedge is smaller than the quantum-size effect. The top valence subband remains a heavy-hole subband. This phenomenon is confirmed by the TE polarization of the laser output and by a blue shift in the measured TM polarized gain spectrum with respect to the TE gain spectrum. It should be noted that a slightly tensile quantum-well laser does not provide the best performance [1] because of the strong valence band mixing. The small separation between the heavy-hole and the light-hole subbands yields a negative heavy-hole effective mass near the band edge and increases the

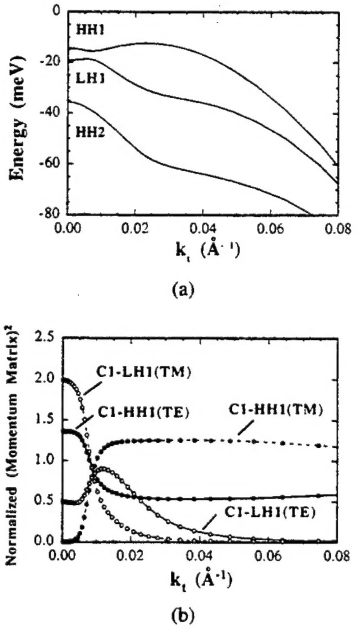

Fig. 5. (a) The valence subband structures for the strained InGaAsP quantum-well laser structure under investigation. The top subband remains heavy-hole-like since the well is only slightly tensile strained. (b) The normalized optical matrix element for both TE and TM polarizations due to the C1-HH1 and C1-LH1 transitions in the strained quantum well.

transparency carrier density. For superior laser performance, a large separation between the heavy-hole and light-hole subbands is desired to take full advantage of the two-dimensional density of states in achieving population inversion. When the two valence subbands are too close, more carriers are wasted in distributing among these subbands instead of contributing to the gain process. Although there has been prediction of some advantages using tensile strained quantum wells [17], [24], [25], such as a higher differential gain and the reduced chirping parameter or linewidth enhancement factor [4]–[6], our choice of the tensile strain in this quantum-well laser does not take advantage of these qualities since the heavy-hole subband remains as the dominant transition path.

In Fig. 6, we show the measured and calculated TE polarized modal gain spectra at three different injection currents, 6, 8, and 10 mA. The carrier densities are determined from the transparency energies which can be obtained at each injection current from the experimental modal gain spectrum. By assuming a bandgap renormalization coefficient C and using the calculated bandstructure, a carrier density which gives the quasi-Fermi level separation ΔF equal to the transparency energy is found. We vary the value of C to match the peak gain wavelength of the 8 mA gain spectrum. The same value of C is then used to determine the carrier densities at the other injection currents. The carrier densities are found to be $N = 2.41$, 2.66, and 2.82×10^{18} cm^{-3}, for the three injection currents, 6, 8, and 10 mA, respectively. The bandgap renormalization coefficient is found to give a bandgap shift of -30 meV for a 2-D carrier density 1×10^{12} cm^{-2}. The Γ for the tested laser is about 0.1, calculated directly from the waveguide theory using the refractive indices and the waveguide dimension d. The experimental and theoretical

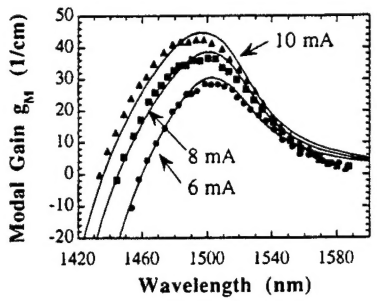

Fig. 6. Our measured modal gain spectra (symbols) below threshold at $I =$ 6, 8, and 10 mA using the Hakki–Paoli method. The theoretical material gain spectrum multiplied by the optical confinement factor is also plotted (solid curves).

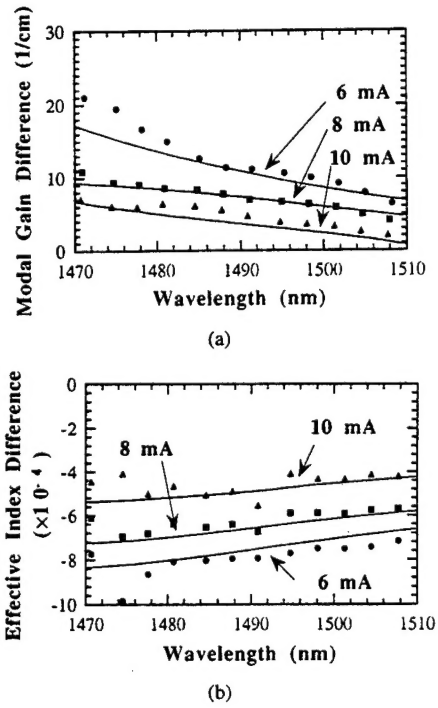

Fig. 7. (a) The measured modal gain difference spectra and (b) the refractive index change at three injection currents $I = 6$, 8, and 10 mA (symbols) are compared with our theoretical results (solid curves).

results agree very well with each other. Note that only two fitting parameters, C and γ, are used, and the experimental spectra are explained very well with the full valence band-mixing model. The slight difference on the low energy side shows that the gain broadening mechanism below the band edge does not follow a Lorentzian lineshape.

Both measured and calculated data of modal gain difference and the induced refractive index change as a function of wavelength are plotted in Fig. 7. The modal gain difference is obtained from the difference of two gain spectra at two nearby current levels, and it tends to increase with increasing photon energy (shorter wavelength). This is due to band filling effects, i.e., the increased carriers tend to pile up at the higher energy levels as the lower levels are already populated. We obtain the differential gain spectra by dividing the curves in Fig. 7(a) by the carrier density difference. The

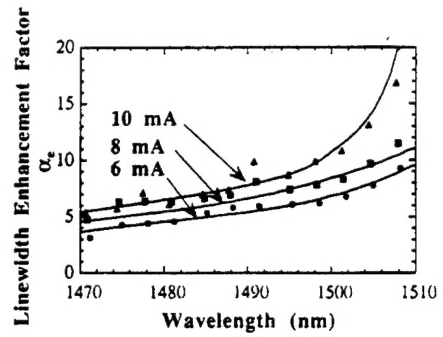

Fig. 8. The linewidth enhancement factor obtained from (25) as the ratio of Fig. 7(a) and (b) is plotted as a function of the optical wavelength. The symbols are experimental data and the solid curves are our theoretical results.

same procedure is used to extract the current-induced change in effective index spectra. The change in the refractive index profile is related to the change in the gain spectrum through a Kramers–Kronig transformation. Our formula (19) is a direct numerical evaluation of the refractive index profile and it automatically takes into account the Kramers–Kronig relation and the scattering broadening mechanism.

In Fig. 8, we show the linewidth enhancement factor α_e, extracted using (25). The theoretical plot using (20) is also shown. The linewidth enhancement factor is proportional to the ratio of the refractive index change per injected carrier concentration and the differential gain profile. Since the refractive index change is roughly constant over the entire wavelength range of interest, the α_e spectrum is determined mainly by the differential gain profile. α_e tends to decrease at shorter wavelengths because of the increased differential gain caused by the band filling effects.

V. Conclusion

Theoretical models and experimental procedures for determining the gain, refractive index and linewidth enhancement factor from the Fabry–Perot peaks and peak shifts in the amplified spontaneous emission spectra of a strained InGaAsP quantum-well laser have been presented. The gain and the refractive index change profiles of a strained quantum-well laser structure can be extracted accurately by taking into account the optical confinement factor. The measured effective refractive index profile agrees with previously reported values [21], after taking into account the waveguide effect and the effective index. The measured refractive index profile is also used to extract the cavity length which agrees very well with the direct observation. Furthermore, accurate monitoring of the differential gain and the Fabry–Perot peak shift with injection current allows measurement of the linewidth enhancement factor, which has a direct impact on the high-speed modulation of semiconductor lasers. The laser tested has a linewidth enhancement factor of approximately 5 at the lasing wavelength, and is comparable to the values cited in the literature. Strain effects can be used to design quantum-well lasers to operate at a lasing wavelength where the linewidth enhancement factor can be minimized. The excellent agreement between our theoretical results and experimental data verifies the material parameters and the quantum-well band structures used in our model. ASE spectroscopy provides an excellent tool for diagnosing a strained quantum-well structure under current injection.

Acknowledgment

The computation time was provided by the National Center for Supercomputing Applications, University of Illinois at Urbana-Champaign.

References

[1] P. J. A. Thijs, L. F. Tiemijer, J. J. M. Binsma, and T. van Dongen, "Progress in long-wavelength strained-layer InGaAs(P) quantum-well semiconductor lasers and amplifiers," *IEEE J. Quantum Electron.*, vol. 30, pp. 477–499, 1994.

[2] P. J. A. Thijs, L. F. Tiemijer, P. I. Kuindersma, J. J. M. Binsma, and T. van Dongen, "High-performance of 1.5 μm wavelength InGaAs-InGaAsP strained quantum-well lasers and amplifiers," *IEEE J. Quantum Electron.*, vol. 27, pp. 1426–1438, 1991.

[3] C. H. Henry, "Theory of the linewidth of semiconductor lasers," *IEEE J. Quantum Electron.*, vol. QE-18, pp. 259–264, 1982.

[4] L. F. Tiemeijer, P. J. A. Thijs, P. J. de Waard, J. J. M. Binsma, and T. v. Dongen, "Dependence of polarization, gain, linewidth enhancement factor, and K factor on the sign of the strain of InGaAs/InP strained-layer multiquantum-well lasers," *Appl. Phys. Lett.*, vol. 58, pp. 2738–2740, 1991.

[5] A. Kimura, M. Nido, S. Murata, J.-I. Shimizu, K. Naniwae, and A. Suzuki, "Strain dependence of the linewidth enhancement factor in long-wavelength tensile- and compressive-strained quantum-well lasers," *IEEE Photon. Technol. Lett.*, vol. 5, pp. 983–986, 1993.

[6] F. Kano, T. Yamanaka, N. Yamamoto, H. Mawatari, Y. Tohmori, and Y. Yoshikuni, "Linewidth enhancement factor in InGaAsP/InP modulation-doped strained multiple-quantum-well lasers," *IEEE J. Quantum Electron.*, vol. 30, pp. 533–537, 1994.

[7] K. Kikuchi, M. Amano, C. E. Zah, and T. P. Lee, "Measurement of differential gain and linewidth enhancement factor of 1.5-μm strained quantum well active layers," *IEEE J. Quantum Electron.*, vol. 30, pp. 571–576, 1994.

[8] D. Ahn and S. L. Chuang, "Optical gain in a strained-layer quantum-well laser," *IEEE J. Quantum Electron.*, vol. 24, pp. 2400–2406, 1988.

[9] E. P. O'Reilly and A. R. Adams, "Band-structure engineering in strained semiconductor lasers," *IEEE J. Quantum Electron.*, vol. 30, pp. 366–379, 1994.

[10] D. Ahn, and S. L. Chuang, "The theory of strained-layer quantum-well lasers with bandgap renormalization," *IEEE J. Quantum Electron.*, vol. 94, pp. 350–365, 1994.

[11] C. S. Chang and S. L. Chuang, "Modeling of strained quantum-well lasers with spin-orbit coupling," *IEEE J. Select. Topics Quantum Electron.*, special issue on semiconductor lasers, vol. 1, pp. 218–229, 1995.

[12] B. W. Hakki and T. L. Paoli, "cw degradation at 300 K of GaAs double-heterostructure junction lasers. II. Electronic gain," *J. Appl. Phys.*, vol. 44, pp. 4113–4119, 1973.

[13] F. Kano, T. Yamanaka, N. Yamamoto, Y. Yoshikuni, H. Mawatari, Y. Tohmori, M. Yamamoto, and K. Yokoyama, "Reduction of linewidth enhancement factor in InGaAsP-InP modulation-doped strained multiple-quantum-well lasers," *IEEE J. Quantum Electron.*, vol. 30, pp. 1553–1559, 1994.

[14] J. M. Luttinger and W. Kohn, "Motion of electrons and holes in perturbed periodic field," *Phys. Rev.*, vol. 97, pp. 869–883, 1955.

[15] G. L. Bir and G. E. Pikus, *Symmetry and Strain-Induced Effects in Semiconductors.* New York: John Wiley, 1974.

[16] K.-H. Hellwege and Landolt-Börnstein, Eds., *Numerical Data and Functional Relationships in Science and Technology.* Berlin: Springer, 1982. New Series, Groups III–V, vol. 17a; Berlin: Springer, 1986, Groups III–V, vol. 22a.

[17] C. S. Chang and S. L. Chuang, "Universal curves for optical-matrix elements of strained quantum wells," *Appl. Phys. Lett.*, vol. 66, pp. 795–797, 1995.

[18] S. L. Chuang, J. O'Gorman, and A. F. J. Levi, "Amplified spontaneous emission and carrier pinning in laser diodes," *IEEE J. Quantum Electron.*, vol. 29, pp. 1631–1639, 1993.

[19] S. L. Chuang, *Physics of Optoelectronic Devices.* New York: Wiley, 1995.
[20] Y. C. Chang, J. N. Schulman, and U. Efron, "Electro-optic effect in semiconductor superlattices," *J. Appl. Phys.*, vol. 62, pp. 4533–4537, 1987.
[21] S. Adachi, "Refractive indices of III–V compounds: Key properties of InGaAsP relevant to device design," *J. Appl. Phys.*, vol. 53, pp. 5863–5869, 1982.
[22] C. G. Van de Walle, "Band lineups and deformation potentials in the model-solid theory," *Phys. Rev. B*, vol. 39, pp. 1871–1883, 1989.
[23] G. Tränkle, E. Lach, A. Forchel, F. Scholz, C. Ell, H. Haug, and G. Weimann, "General relation between bandgap renormalization and carrier density in two-dimensional electron-hole plasmas," *Phys. Rev. B*, vol. 36, pp. 6712–6714, 1987.
[24] G. Jones and E. P. O'Reilly, "Improved performance of long-wavelength strained bulk-like semiconductor lasers," *IEEE J. Quantum Electron.*, vol. 29, pp. 1344–1354, 1993.
[25] T. Tütken, B. J. Hawdon, M. Zimmermann, I. A. Hangleiter, and V. Härle, "Improved modulator characteristics using tensile strain in long-wavelength InGaAs/InGaAsP multiple quantum wells," *Appl. Phys. Lett.*, vol. 64, pp. 403–404, 1994.

Chih-Sheng Chang was born in Hualien, Taiwan, on Nov. 3, 1964. He received the B.S. and M.S. degrees in electrical engineering from National Taiwan University, Taipei, Taiwan, in 1986 and 1990, respectively and is currently working toward the Ph.D. degree in electrical engineering as a Research and Teaching Assistant in the Department of Electrical and Computer Engineering, University of Illinois at Urbana-Champaign.

His research interests include quantum-well optoelectronic devices, optical rectification theories, and optical waveguides.

Shun Lien Chuang (S'78–M'82–SM'88) was born in Taiwan in 1954. He received the B.S. degree in electrical engineering from National Taiwan University in 1976, and the M.S., E.E., and Ph.D. degrees in electrical engineering from the Massachusetts Institute of Technology in 1980, 1981, and 1983, respectively.

While in graduate school, he held research and teaching assistantships, and also served as a recitation instructor. In 1983, he joined the Department of Electrical and Computer Engineering at the University of Illinois at Urbana-Champaign, where he is currently a Professor. He was a resident visitor at AT&T Bell Laboratories, Holmdel, NJ, in 1989. He was a consultant at Bellcore and Polaroid in 1991, at AT&T Bell Laboratories, Murray Hill, NJ, in 1992, and a Senior Visiting Professor at SONY Research Center, Japan, in the summer of 1995. He was also an Associate at the Center for Advanced Study at the University of Illinois in Fall 1995. He is conducting research on strained quantum-well semiconductor lasers and electrooptic modulators and nonlinear optics. he developed a graduate course on integrated optics and optoelectronics. He has been cited several times for Excellence in Teaching.

Dr. Chuang is a member of the Optical Society of America and American Physical Society. He has been awarded a fellowship from the Japan Society for the Promotion of Science and will visit University of Tokyo in 1996. He is the author of *Physics of Optoelectronic Devices* (Wiley) in the Pure and Applied Optics Series. He was a co-editor for a special issue in *Journal of Optical Society of America B* on Terahertz Generation, Physics and Applications published in Dec. 1994. He was invited to give talks at many conferences including the American Physical Society March Meeting, Optical Society of America Annual Meeting, and Integrated Photonics Research.

Jeffrey R. Minch was born in Schnectady, NY, in 1971. He received the B.S. degree in electrical engineering from Cornell University, Ithaca, NY, in 1993, the M.S. degree in electrical engineering from the University of Illinois at Urbana-Champaign in 1995, where he is currently working toward the Ph.D. degree.

His research interests include quantum and optical electronic devices, especially semiconductor lasers.

Wei-chiao W. Fang was born in Cambridge, MA, in 1970. He received the B.S. degree in electrical engineering from Cornell University in 1992 and the M.S. degree in electrical and computer engineering from the University of Illinois at Urbana-Champaign in 1993, where he is presently working towards the Ph.D. degreen.

His research interest includes quantum and optical electronics, with a particular focus on semiconductor lasers, optical modulators and detectors. He received the FMC Education Fund Fellowship in 1993 and the Frederic T. and Edith F. Mavis Fellowship Award in 1994. He has been supported by the AT&T Foundation Fellowship since 1994. He conducted research at AT&T Bell Laboratories, Murray Hill, NJ, during the winter of 1993 and the summer of 1994.

Y. K. Chen, photograph and biography not available at the time of publication.

T. Tanbun-Ek, photograph and biography not available at the time of publication.